Measurement Notes

Note 57

April 2002

MEASUREMENT AND EVALUATION OF ARTIFICIAL DIELECTRIC MATERIAL

Charles A. Frost
Pulse Power Physics, Inc

Abstract

This note describes measurements of dielectric parameters for artificial dielectric materials using picosecond time domain instrumentation. The time domain data is transformed to yield frequency dependent permittivity and loss factor. Artificial dielectric materials are of interest for lightweight dielectric lenses for ultra-wideband and wideband sources and antennas. Such lightweight antennas are useful for airborne and space applications.

1. INTRODUCTION

This report documents research performed to evaluate the electromagnatic performance of commercially available artificial dielectric materials. Two materials were determined to be suitable for UWB (ultra-wideband) and WB (wideband) microwave sources and antennas. The materials displayed minimal pulse dispersion. The permittivity showed little frequency dependence over the range of 3 to 23 GHz. Evaluation was accomplished by Fourier transforming experimentally acquired time domain data to the frequency domain to obtain complex dielectric properties of the material as a function of frequency. The basic analysis method was described in [1], but the method had not previously been applied to the study of artificial dielectric materials. We extended the measurement technique of [1] to the case of free propagating waves using radiating antennas and compared to results obtained with a bounded wave transmission line measurement.

We fabricated test samples from commercial artificial dielectric material and performed time domain pulse transmission measurements. Two types of artificial dielectric material were studied and compared to polyethylene. One type was based on metal particles in a dielectric matrix. The other type used high permittivity material in a closed cell foam. Polarization effects (anisotropy) were addressed by measurements with the electric field along and perpendicular to the optic axis of the sample. The measurements were performed at low level using time domain metrology with a Tektronix 11801 sampling digitizer and picosecond pulse generator. Dielectric lens focused TEM horn antennas were used to launch and receive the electromagnetic impulse. The measurements performed under this effort complement previous time domain measurements [2] which were performed in development of lens antennas for phased array impulse sources. The current research effort extended results to the frequency domain and study of polarization effects. A TEM cell was also developed for this project, and bounded wave data was compared to freely propagating wave data [2] acquired with the two antenna method. All measurements were performed at facilities of Pulse Power Physics, Inc.

2. TIME DOMAIN MEASUREMENTS WITH FREELY PROPAGATING WAVES

Artificial dielectric material was characterized using a free propagating wave measurement with a pair of lensed horn antennas. Pulse transmission measurements were performed to characterize dielectric materials using the experimental setup shown by figure 1 with the small TEM horn antennas separated by 48 inches. The Tektronix model 11801 sampling oscilloscope recorded the signal from the receiving antenna. The fast risetime pulser and transmit antenna produced a radiated impulse with a full width at half maximum less than 40 ps.

The permittivity for the material was determined by measuring the increase in pulse propagation delay when passing the pulse through slabs of dielectric. The measurement also allowed determination of the dispersion of the dielectric material. Dispersion occurs for dielectric materials which have a frequency dependent wave speed. A narrow impulse is spread out due to the dispersion.

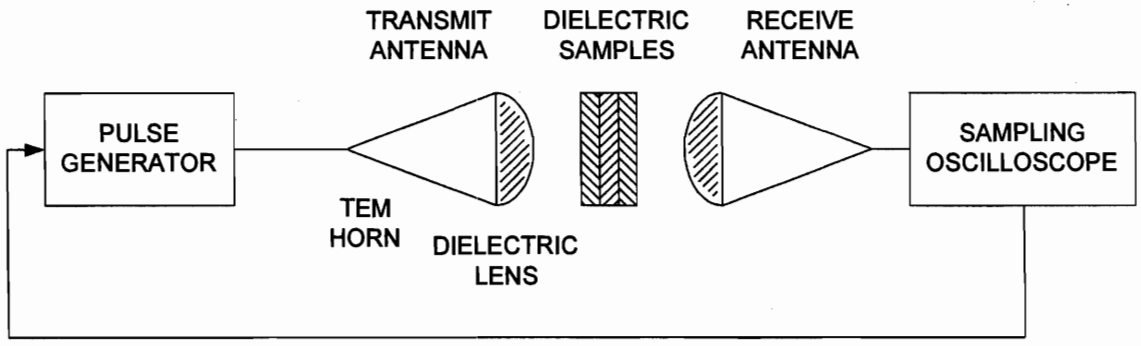

Figure 1. Experimental setup used to measure dielectric properties of artificial dielectric material

We first discuss measurements performed on C-Stock 265 material which was supplied by Cuming Corporation. C-Stock 265 is a rigid, lightweight, filled plastic material that functions as an artificial dielectric material; in other words, it exhibits controlled permittivity and low dissipation factor at microwave frequencies. C-Stock 265 was supplied in cast square plates. The material was developed for application in making microwave lenses, radomes, and other antenna parts, particularly for aircraft applications. Its principal advantage is that it is lower in density than conventional materials of equal permittivity. According to the manufacturer, the material has not been used previously for time domain applications, and there is no data available on dispersion in ultra-wide bandwidth applications.

The standard form of C-Stock 265 is based on epoxy plastic resin and glass microspheres combined to form syntactic foam, loaded with metallic powder to achieve the desired electrical behavior. The material is strong enough to serve as the core of load-bearing composite sandwich panels. The C-Stock 265 material was supplied as 12-inch square cast plates. The plates had a thickness of 2.72 cm. Four of these plates were used. A measurement was made with a reference air path, and then with dielectric samples inserted into the propagation path. Figure 2 shows an overlay plot of the received signal waveforms with zero through four artificial dielectric plates inserted. The peak of the pulse is shifted to the right by a 58 ps delay time with the addition of each additional dielectric slab. The pulse is also broadened due to dispersion.

There is a drop in amplitude due to reflection loss at entry and exit from the dielectric material. This is due to reflection from the discontinuity at the air-dielectric interface. The Fresnel loss term was calculated to be 6% for the C-265 material. The reflection loss can be seen as a drop in amplitude for all of the delayed waveforms relative to the air path which suffers no Fresnel loss. There is also a slight additional drop in amplitude and increase in pulsewidth with increasing propagation distance through the material due to high frequency attenuation and dispersion.

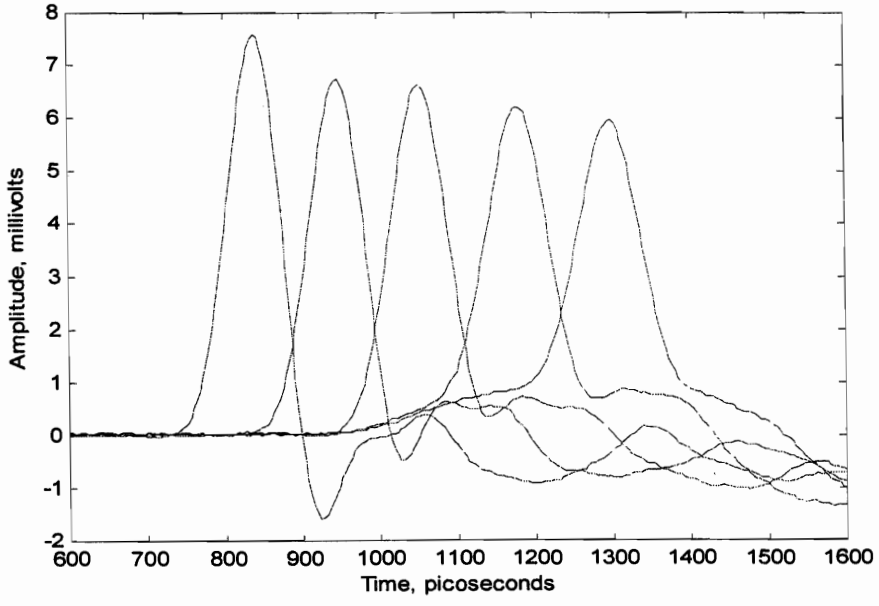

Figure 2. Overlay of received pulse after propagation through slabs of artificial dielectric sample length

The propagation delay time Δt relative to the reference air path was measured for each propagation length using the digitizer built-in measurement functions. The delay time was measured from the peak of the impulse. The pulse width τ (full width at half of maximum or FWHM) was also measured for each waveform. Table 1 lists the measured values for Δt and τ as a function of the total material sample length Δl. The data of table 1 indicate that Δt is approximately proportional to Δl. The deviation from linearity is caused by dispersion which broadens the pulse with increasing propagation distance causing the peak to shift beyond the linear slope.

The dispersion $\Delta\tau$ can be quantified by normalization of the pulse width τ to the pulse width τ_o for the reference air path. This is calculated by the formula, $\Delta\tau = \sqrt{\tau^2 - \tau_0^2}$. If we divide $\Delta\tau$ by the sample length Δl, we get the dispersion per unit length. Table 1 lists Δt, τ, $\Delta\tau$, and $\Delta\tau/\Delta l$, all as functions of Δl. It can be seen that the dispersion is approximately 10% of the propagation delay.

Table 1
Type C-265 Artificial Dielectric Measurements
(Time Domain Data)

Sample Length Δl cm	Propagation Delay Δt ps	Pulsewidth τ ps	Dispersion $\Delta\tau = \sqrt{\tau^2 - \tau_0^2}$ ps	Dispersion per unit length $\Delta\tau/\Delta l$ ps/cm
0.00	0	38.7	0.0	--
2.72	54	39.5	7.91	2.9
5.44	108	43.0	18.7	3.4
8.15	171	47.2	27.0	3.3
10.87	231	50.8	32.9	3.0

From optics the refractive index n of a material is defined as the ratio of the wave speed in vacuum to the wave speed in the material. We calculate the refractive index as $n = 1 + c\,\Delta t/\Delta l$, where c is the speed of light in vacuum (30 cm/ns). The factor 1 occurs because the total path length is fixed, and the samples are merely inserted replacing air with dielectric material. We calculate a value of 1.64 for the refractive index n

using the longest propagation distance, which was 10.87 cm. We calculate a value of 2.68 for the relative permittivity $\varepsilon_R = \frac{\varepsilon}{\varepsilon_o}$, which is calculated as the square of the refractive index. In the simple time domain representation employed here, the calculated value of n depended on the propagation length due to the effect of dispersion. In the following section we use a frequency domain representation of the refractive index to better describe this effect.

We performed similar measurements with a 10.34 cm thick slab of polyethylene dielectric to check the accuracy of our measurements. Polyethylene was chosen for the calibration check because it is known to have a permittivity of 2.26 which is almost independent of frequency [3]. We calculate 1.51 for the refractive index and 2.28 for the relative permittivity based on the measured values of Δt and Δl. The measured pulse broadening for polyethylene gives a value of 0.54 ps/cm for the dispersion per unit length. The close agreement of our measurement with the known value for polyethylene gives us confidence in the accuracy of the method.

We also performed measurements on a different type of artificial dielectric material. The C-Cast 236 material is a thermosetting epoxy compound which is loaded with hollow glass microspheres to form a syntactic foam which has a effective permittivity higher than air but lower than the epoxy base. The C-Cast 236 does not include the metallic particle filler but is much lighter than the C-Stock 265 and can be mixed by the user for pouring into molds rather than machining to shape. We prepared an 8-inch diameter sample of the C-236 material by mixing the two components and pouring into a cylindrical mold. The material was vacuum degassed and heat cured at 150°C. The sample was then machined to a thickness of 2.44 cm for accurate measurement.

For the C-236 material, we calculate 1.43 for the refractive index and 2.04 for the relative permittivity based on the measured values of Δt and Δl. The pulse broadening for C-236 gives a value of 3.4 ps/cm for the dispersion per unit length. Table 2 summarizes the dielectric properties computed from the measured data for the three materials studied. Table 2 also shows the material mass density which was determined by weighing the samples with a digital scale and measuring dimensions with dial calipers.

Table 2. Dielectric Material Properties from Time Domain Measurement

Material	n	ε_R	$\Delta\tau/\Delta l$ ps/cm	Density g/cm^3
Polyethylene	1.51	2.28	0.5	0.95
C-265	1.64	2.68	3.0	0.73
C-236	1.43	2.04	3.4	0.67

3. FREQUENCY DOMAIN ANALYSIS

The literature contains a number of references on determination of complex properties by transformation of time domain data to the frequency domain. Shortly after the advent of the sampling oscilloscope, Nicholson and Ross [4] developed a technique to extract the complex permittivity and permeability from Fourier transformed time domain signals in a coaxial transmission line fixture. Their method requires measurement of both the reflected and transmitted signal. More recently, Courtney et.al. [5] improved the method to avoid the need to normalize to a reference plane. Non-perturbing D-dot probes were used to sample the incident and transmitted signals. Both of these methods determine both the relative permittivity ($\varepsilon_R = \frac{\varepsilon}{\varepsilon_o}$) and the relative permeability ($\mu_R = \frac{\mu}{\mu_o}$), simultaneously.

For non-magnetic materials a better signal-to-noise ratio can be obtained by forcing the value of μ_R to 1 leaving one free parameter to be determined, rather than two. With non-magnetic materials the complex permittivity can be exactly determined from the transmitted waveform and a normalization waveform. The reflected signal is not required. For example, Aurand [6] used this method to measure the complex permittivity of sand and concrete walls using freely propagating waves between two ultra-wideband antennas. The data was corrected for Fresnel loss at the interface. A related approach reported by Farr and Frost [1,7] employed two samples of the unknown material with different lengths. The Fresnel losses, which were the same for the two samples, canceled out of the analysis. This method avoided the correction for Fresnel losses.

The Farr/Frost method [1,7] was originally performed in a coaxial transmission line. The present work extends this technique to the freely

propagating waves between two antennas. In addition, a planar TEM cell test fixture was fabricated specifically for this measurement, and results from the freely propagating and bounded wave measurements were compared.

We will now describe the basis for determination of complex dielectric parameters by transformation of time domain data into the frequency domain. The time domain data were acquired as described in section 2 using the instrumentation setup of figure 1.

The measurement technique is based on two separate transmission measurements over the same path length. For the first measurement, we record a transmitted voltage waveform A(t) passing through a material sample of length ℓ_1 of the unknown dielectric. For the second measurement, we record a transmitted voltage waveform B(t) with the sample length increased to ℓ_2. An identical time domain pulse is employed for both measurements. The transfer function T(f) for transmission through the difference in length ($\ell_2 - \ell_1$) of the unknown material is computed by taking the ratio of the two transmitted signals in the frequency domain as shown by equation (1).

$$T(f) = \frac{FFT[B(t)]}{FFT[A(t)]} \qquad (1)$$

We can relate the complex dielectric properties of the material to the measured transfer function T(f) through the theory of time harmonic traveling waves. This theory is strictly correct for the case of TEM wave propagation in the coaxial transmission line and approximately correct for spherical waves in the two antenna measurement. For non-magnetic material, the transfer function is given by

$$T(f) = e^{-j\frac{2\pi f}{c}(\ell_2-\ell_1)(n-1)} \qquad (2)$$

where we have assumed harmonic time dependence and ($\ell_2 - \ell_1$) is the difference in length between the two samples, f is the frequency in Hertz, c is the speed of light in vacuum, and n is the refactive index which is the ratio of c to the wave velocity in the material sample. Note that the Fresnel losses at the dielectric interfaces are identical for the two measurements, so that they cancel out of the analysis. Equation (2) ignores secondary reflections which can be time-gated out of the measurement.

To determine the relative permittivity, we first compute T(f) from the measured time domain transmission waveforms A(t) and B(t) using equation (1). We then solve equation (2) for the frequency dependent index of refraction n(f) by taking logarithms.

$$n(f) = \frac{jc}{2\pi f(\ell_2 - \ell_1)} \ell n[T(f)] + 1 \tag{3}$$

We must take care to properly handle the logarithm of the complex function T(f). In particular, it is necessary to time shift the retarded waveform B(t) prior to Fourier transformation in order to prevent phase wrapping of the function T(f). The time shift must then be converted to a linear phase term which is reinserted in equation (3). We note that n(f) is a complex valued function of frequency, and by convention the real and imaginary parts are defined by

$$n(f) = n'(f) - jn''(f) \tag{4}$$

where n′ is the real part of n which is associated with phase shift and n″ is associated with the exponential decay of amplitude with propagation distance. It was pointed out in [6] that analysis can be simplified and the difficulties of taking the logarithm of the complex function T(f) can be avoided by separation into phase and amplitude terms. We employ this simplification with no loss of generality to obtain the real part of the refractive index as

$$n'(f) = 1 - \frac{c}{2\pi f(\ell_2 - \ell_1)} PHASE[T(f)] \tag{5}$$

where the phase which is measured in radians must be unwrapped prior to use in equation (5).

We define the attenuation factor AF(f), as the attenuation per unit length in decibels. This can be conveniently calculated from

$$AF(f) = \frac{20\log_{10}}{(\ell_2 - \ell_1)} MAGNITUDE[T(f)] \tag{6}$$

where the logarithm is to the base 10. Alternatively, the exponential decay constant $\alpha(f)$ expressed in Nepers per unit length can be calculated by taking the natural logarithm instead of the common logarithm.

The frequency dependent relative permittivity $\varepsilon_R(f) = \frac{\varepsilon(f)}{\varepsilon_o}$ is calculated by squaring the relative permittivity n. The permittivity and attenuation factor fully express the frequency dependent performance of the dielectric material in that the phase shift and attenuation are readily calculable for propagation through any length of the material. The pulse dispersion, which was discussed in section 2, can also be predicted for any assumed pulse shape from these parameters. The reader is referred to [1] for more details on the basis of this method. We will now discuss the computation of the complex dielectric properties of several materials from the measured time domain data using the described method.

Time domain data was collected using the experimental setup shown by figure 1 with a total path length of 48 inches between the two TEM horn antennas. The two experimentally measured time domain waveforms each consisted of a time sequence of 5120 equally spaced sampling points. The Tektronix model 11801 digitizer records were read out and converted to ASCII computer files using Tektronix Docuwave software. Data processing was performed using MATLAB software to implement the mathematical operations given by equations (1) through (6). The resulting point sequences were plotted as graphical output. We present a set of seven graphs for each material studied. These consist of the time domain waveforms A(t) and Bt). At two horizontal resolutions, the magnitude and phase of the transfer function T(f), the real part n'(f) of the refractive index of n(f), the permittivity ε_R(f), and the attenuation factor AF(f) in db/cm.

Two analysis methods were compared. For both methods, the transfer function T(f) for propagation through a differential length ($\ell_2 - \ell_1$) of material is first calculated from the time sequence using equation (1). In the first method, equation (3) was solved to give the complex valued refractive index n which was then squared to obtain the permittivity. The imaginary part n" was used to compute the attenuation factor. In the second method, the transfer function T(f) was expressed in terms of phase and magnitude using the MATLAB built-in functions. Equation (5) was used to compute the real part of the refractive index from the phase. Equation (6) was used to compute the attenuation factor from the magnitude. The relative permittivity ε_R was computed as the square of the refractive index. Both of the two methods gave similar results, but the second method was found to be more stable numerically and did not require shifting of the time domain data. For this reason, we analyzed all of the data using the second method.

We begin with analysis of data collected with the type 265 artificial dielectric, since this material appeared to be the most useful for application to dielectric lenses for ultra-wideband applications. Figure 3 shows the time domain data resulting from propagating the radiated pulse through two different lengths of the material. Two traces are overlaid on figure 3. The first pulse in time will be referred to as waveform A(t). This is the pulse propagated through the shorter sample which had a thickness ℓ_1 of 2.72 cm. The second pulse on figure 3 corresponds to the pulse which propagated through the longer of the two samples which had a thickness ℓ_2 of 10.87 cm. We refer to the second pulse as waveform B(t). The differential path length through the material ($\ell_2 - \ell_1$) was 8.15 cm. Both waveforms show a narrow impulse with an amplitude of approximately 6 X 10^{-3} volts. The later waveform is broadened and slightly reduced in amplitude due to the passage through the additional length ($\ell_2 - \ell_1$) of material.

Figure 4 shows the time domain data at a finer time resolution. The measured time delay Δt between the two peaks is 177 ps. We can directly compute the refractive index n from the time domain data using

$$n = 1 + \frac{c\Delta t}{(\ell_2 - \ell_1)} \qquad (7)$$

Equation (7) gives a value of 1.65 for the refractive index calculated directly from the time domain data. The relative permittivity calculated as the square of n is 2.73 for the type 265 material. The time domain calculation gives a single number corresponding to the mean value over the frequency range contained in the exciting pulse. To get the frequency dependence of n, we Fourier transform into the frequency domain.

Before Fourier transforming the time domain sequence into the frequency domain, it is necessary to window the data to bring the left-hand and right-hand end points into correspondence. This makes the data appear to be part of a periodic sequence. We have chosen to window with a cosine taper over 10% and 20% of the total sequence length on the left-hand and right-hand side, respectively. The data of figure 3 shows very little change with this windowing since it is already near zero at both ends of the range.

Next, we calculate the transfer function T(f) corresponding to propagation through the differentical length ($\ell_2 - \ell_1$) by taking the frequency domain ratio of the Fourier transform of B(t) to the Fourier transform of A(t) using equation (1). Figures 5 and 6 show the magnitude and phase of the computed transfer function T(f). The transfer function contains all the

information available about the dielectric properties of the material. The phase of the transfer function has been unwrapped using the MATLAB built-in function. Figure 6 indicates that the phase is approximately linear with frequency over the range of 3 to 23 GHz with some deviation outside this range. Close examination of figure 6 indicates slight deviation from linear phase which is the result of dispersion due to frequency dependent wave speed. The magnitude is well behaved over the range of 3 to 23 GHz showing a uniform falloff from unity with increasing frequency. At the high and low ends of the frequency span we see anomalous behavior in the magnitude which is an artifact of the measurement.

Figure 7 shows the real part of the refractive index which is calculated from the unwrapped phase data of figure 6 using equation (5). The data is plotted as a function of frequency over the range of 3 to 23 GHz. The refractive index is nearly constant with frequency with a mean value of 1.65 which matches the value obtained from time domain calculation using equation (7). A least squares linear fit to the data is plotted in figure 5, and the slope and intercept values are displayed on the figure. There is a slight decrease in n'(f) with increasing frequency.

Figure 8 plots the relative permittivity $\varepsilon_R(f)$ which is calculated as the square of the refractive index. The straight line fit through the data points is also plotted on the figure. The permittivity has a mean value of 2.72 with a slight decrease in value with increasing frequency. Figure 9 shows the attenuation factor AF(f) which is calculated from the magnitude data of figure 5 using equation (6). The attenuation factor in decibels per unit length shows a near linear increase with frequency.

The results plotted in Figures 3 through 9 illustrate the application of the Fourier transform analysis method to the two antenna time domain radiated wave data to determine complex dielectric properties as a function of frequency. The results for the type 265 artificial dielectric material are encouraging in that they show a permittivity which is relatively constant with frequency over the range of interest for many of the UWB applications. The attenuation factor may be more of a concern, however the measurement method is of limited accuracy in determining attenuation factor. This will be discussed in the following sections.

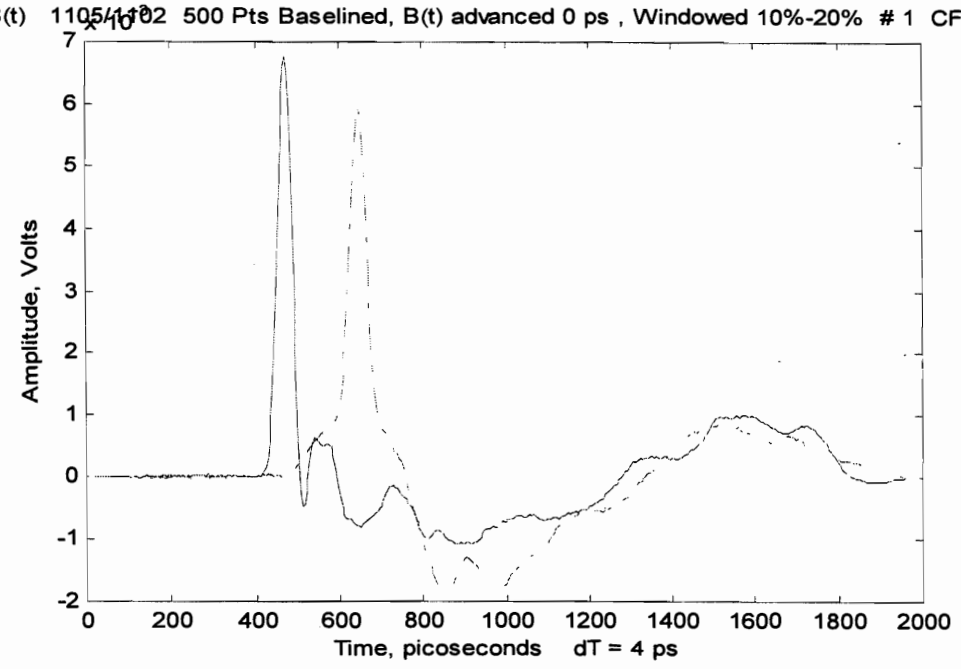

Figure 3. Time domain transmission waveforms A(t) and B(t) for propagation through lengths ℓ_1 and ℓ_2 of type-265 artificial dielectric material between TEM-horn antennas

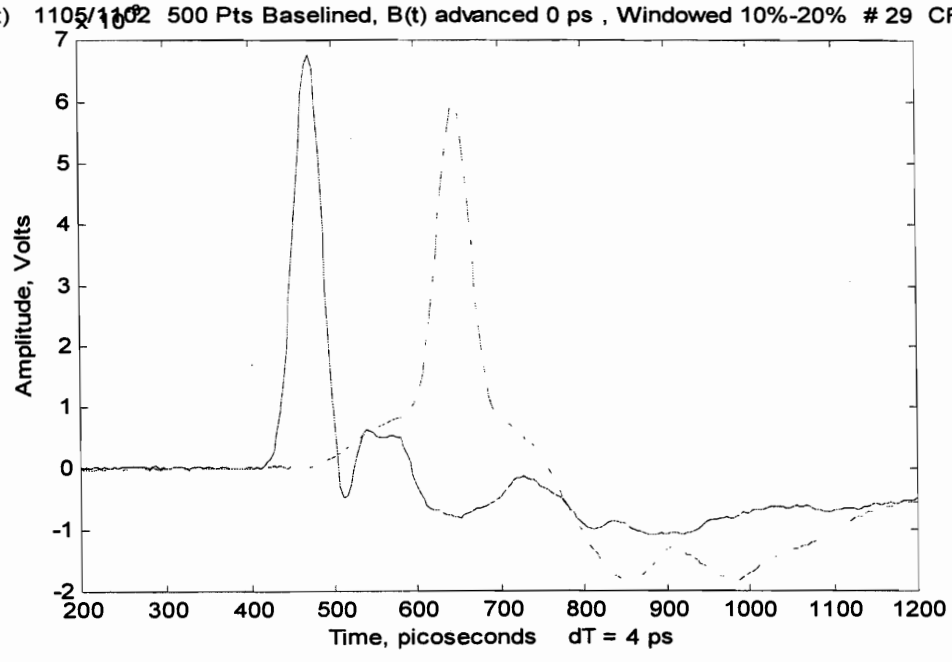

Figure 4. Time domain transmission waveforms A(t) and B(t) for propagation through lengths ℓ_1 and ℓ_2 of type-265 artificial dielectric material between TEM-horn antennas at finer resolution

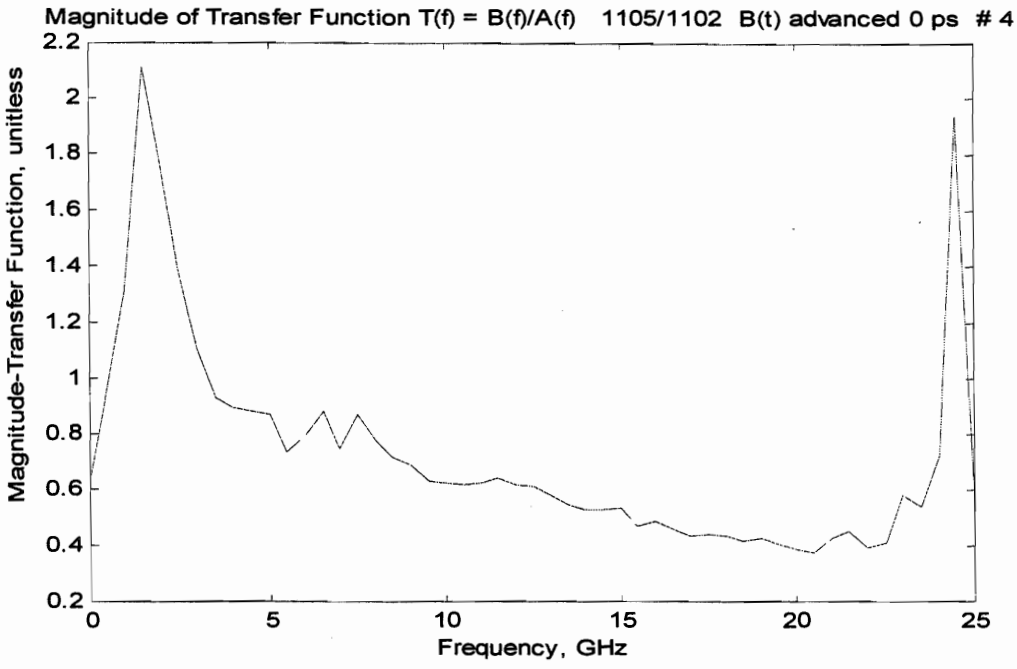

Figure 5. Magnitude of transfer function for propagation through differential length ($\ell_2 - \ell_1$) of type-265 artificial dielectric material between TEM-horn antennas

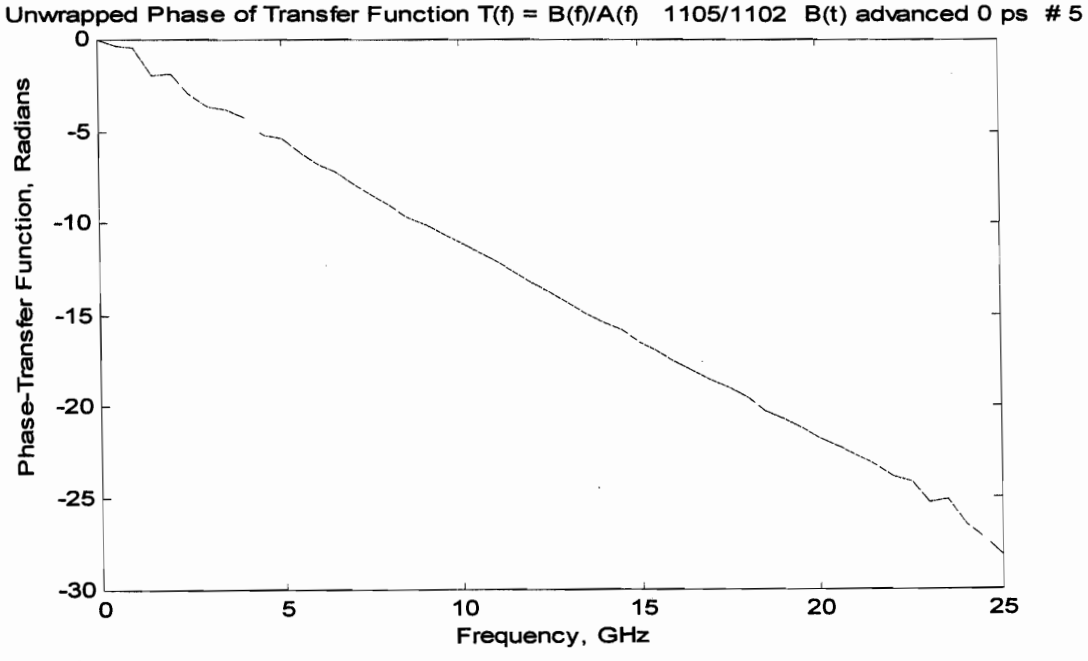

Figure 6. Phase of transfer function for propagation through differential length ($\ell_2 - \ell_1$) of type-265 artificial dielectric material between TEM-horn antennas

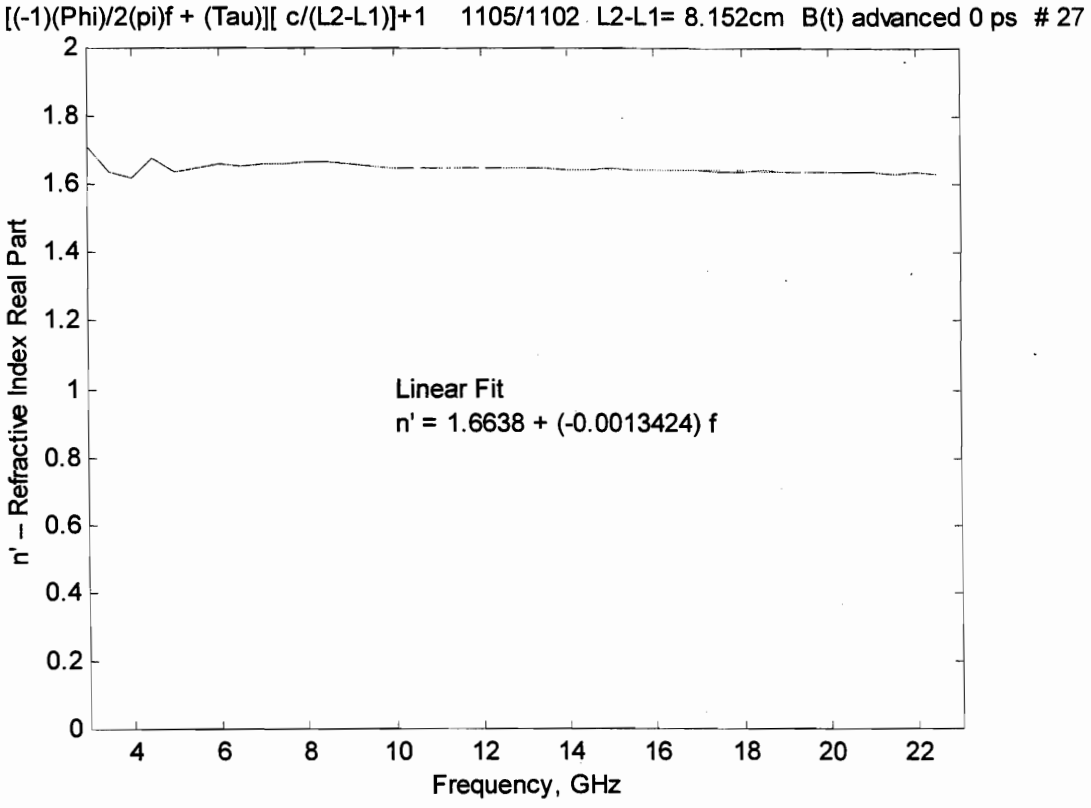

Figure 7. Real part of refractive index for type-265 artificial dielectric material calculated from time domain two antenna measurement

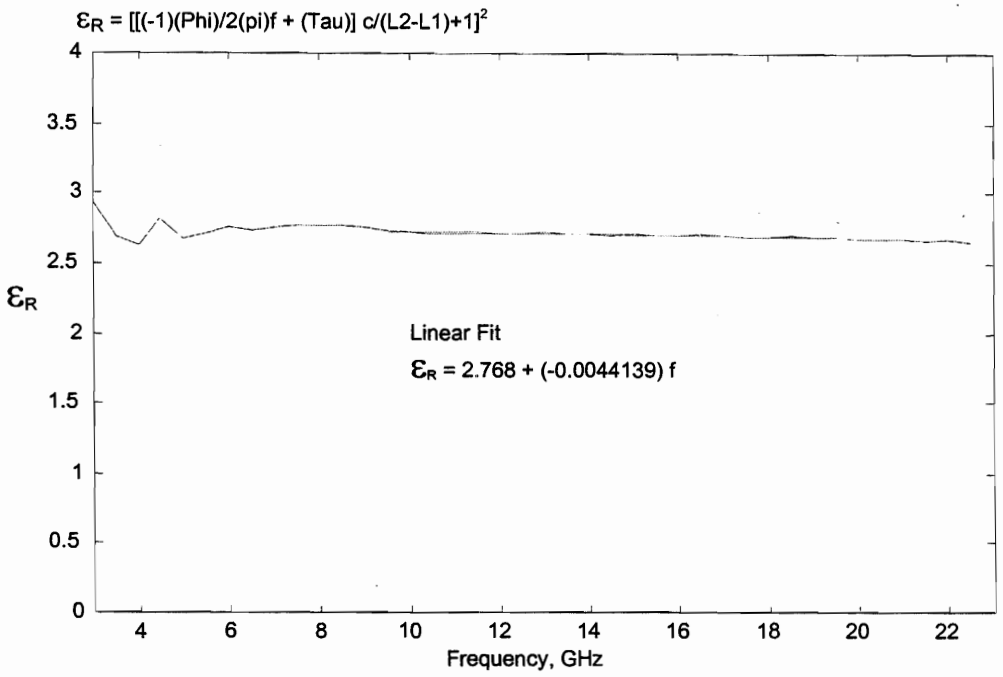

Figure 8. Relative permittivity for type-265 artificial dielectric material calculated from time domain two antenna measurement

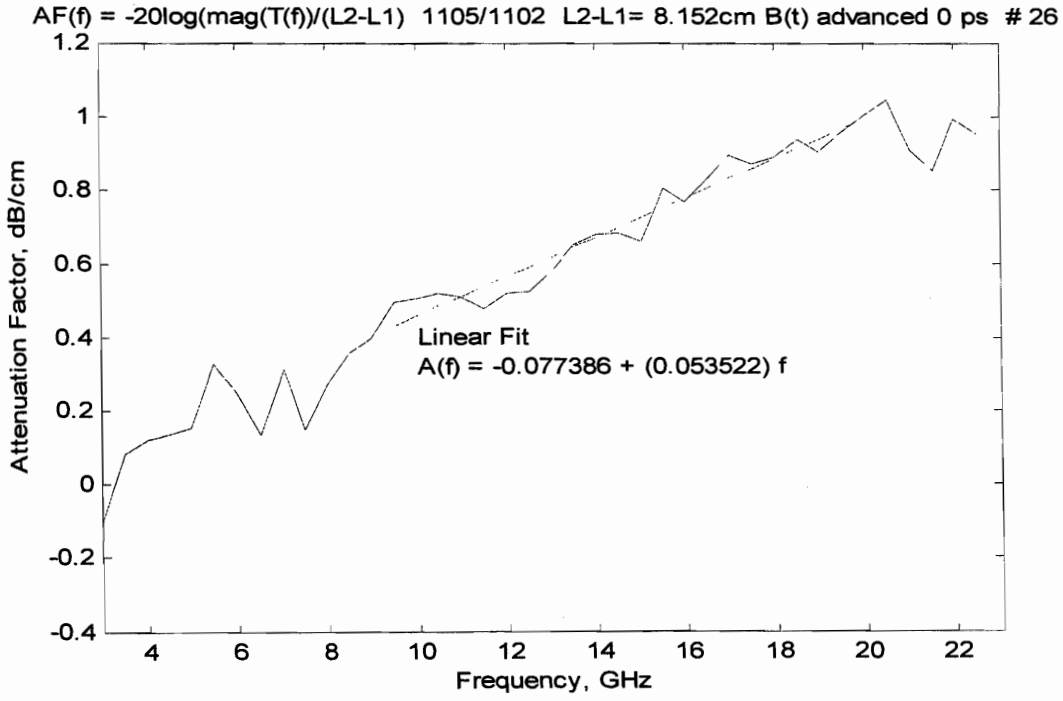

Figure 9. Attenuation factor for type-265 artificial dielectric material calculated from time domain two antenna measurement

The same Fourier transform analysis technique was applied to the two antenna time domain transmission data obtained with type 236 artificial dielectric material sample with a differential sample length ($\ell_2 - \ell_1$) of 2.44 cm. Figures 10 through 16 show the resulting data set for the type 236 material. The time shift measured from figure 11 was 35 ps which gives a value of 1.43 for the refractive index through equation (7). A value of 2.04 is calculated for the relative permittivity. Figures 12 and 13 show a well behaved transfer function T(f) with a magnitude near unity and linear phase delay with frequency over the range of 3 to 23 GHz. Figures 14 and 15 show that the refractive index and relative permittivity are almost independent of frequency with mean values of 1.42 and 2.03 which match the time domain calculations. Figure 16 shows that the attenuation per unit length increases with frequency but is somewhat smaller than measured for the type 265 material.

As a check on accuracy of the technique we measured a reference material, polyethylene, which is known to have a refractive index of 1.50 which is almost constant over the frequency range employed here [3]. Figures 17 through 23 show the corresponding data set for polyethylene material using a differential sample length ($\ell_2 - \ell_1$) of 10.34 cm. The time domain data of figure 18 shows a time delay of 176 ps between the two peaks which gives a refractive index of 1.51 and relative permittivity of 2.28.

The transfer function T(f) shows a highly linear phase (see figure 20) and a magnitude near unity (see figure 19) across the frequency range of 5 to 20 GHz. The refractive index shown by figure 21 is flat with frequency having a mean value of 1.51, while the relative permittivity shown by figure 22 is also flat with frequency with a mean value of 2.28. These values exactly match the values calculated directly from the time domain data and are in excellent agreement with the published values of [3]. As expected, the attenuation factor for this low loss dielectric is near zero for 5 to 23 GHz.

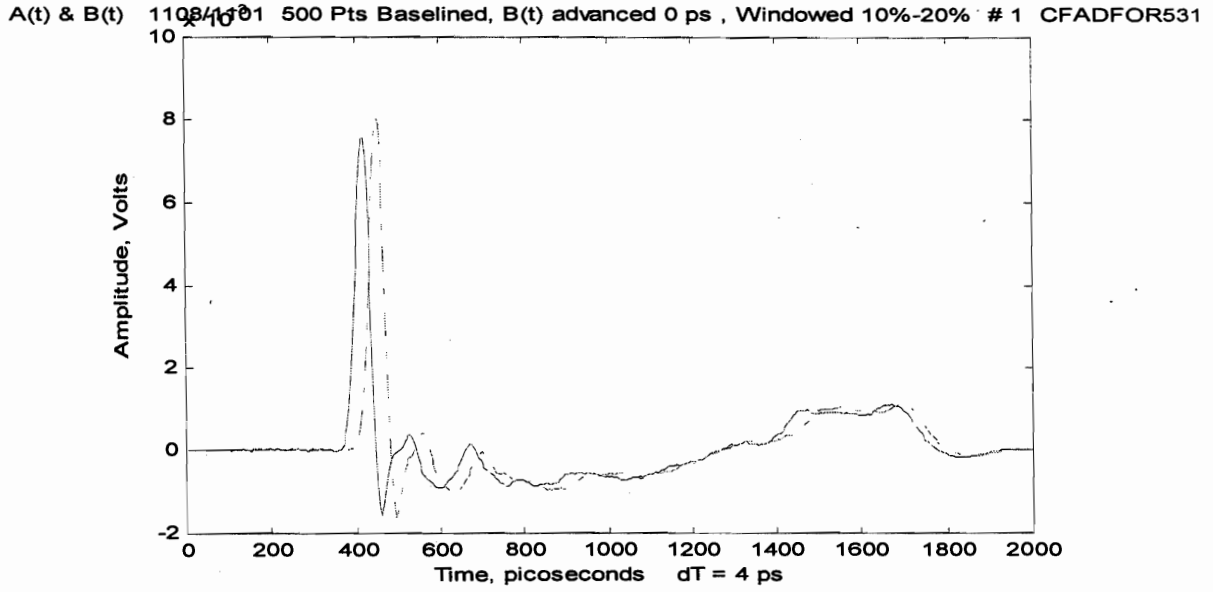

Figure 10. Time domain transmission waveforms A(t) and B(t) for propagation through lengths ℓ_1 and ℓ_2 of type-236 artificial dielectric material between TEM-horn antennas

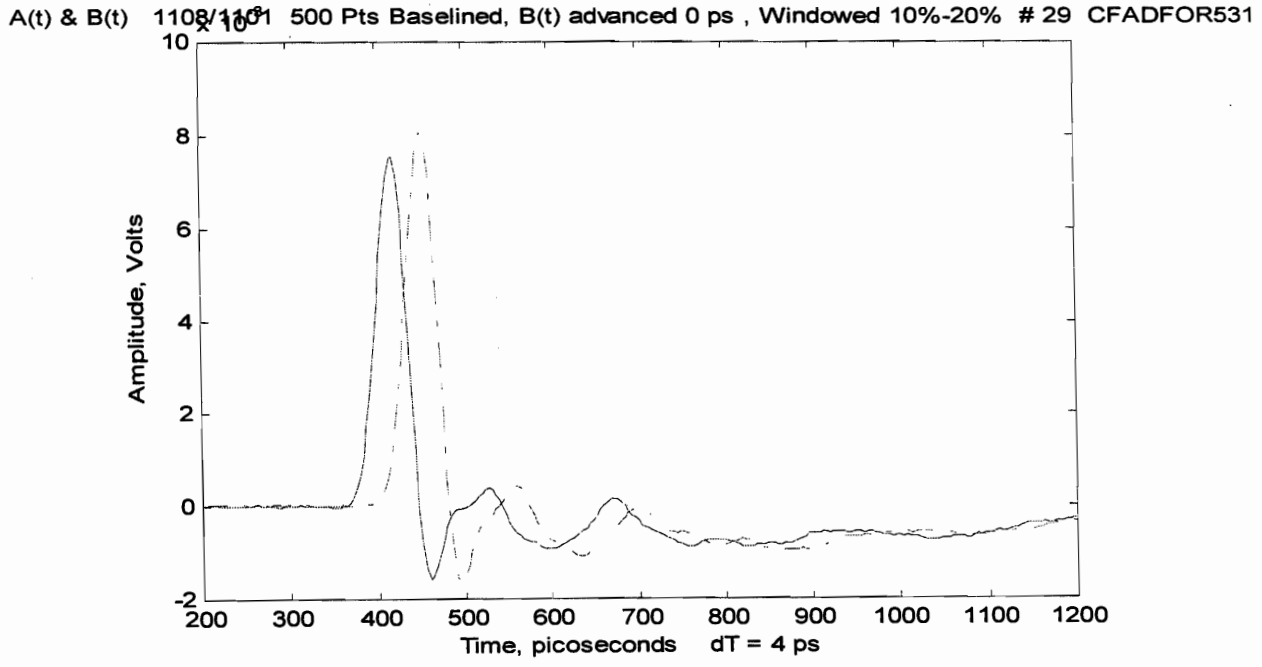

Figure 11. Time domain transmission waveforms A(t) and B(t) for propagation through lengths ℓ_1 and ℓ_2 of type-236 artificial dielectric material between TEM-horn antennas at finer resolution

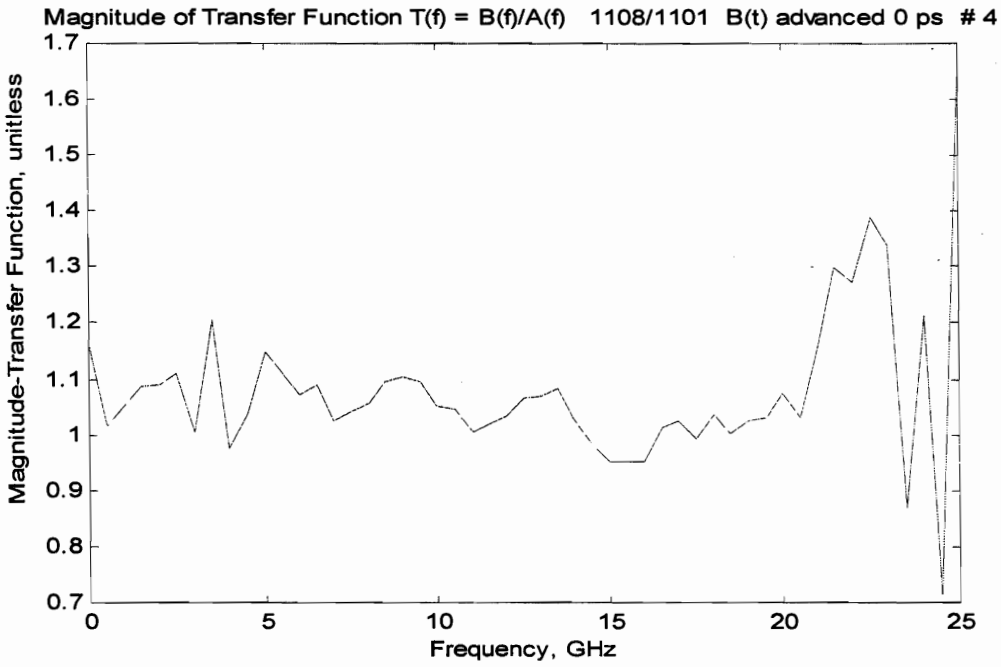

Figure 12. Magnitude of transfer function for propagation through differential length ($\ell_2 - \ell_1$) of type-236 artificial dielectric material between TEM-horn antennas

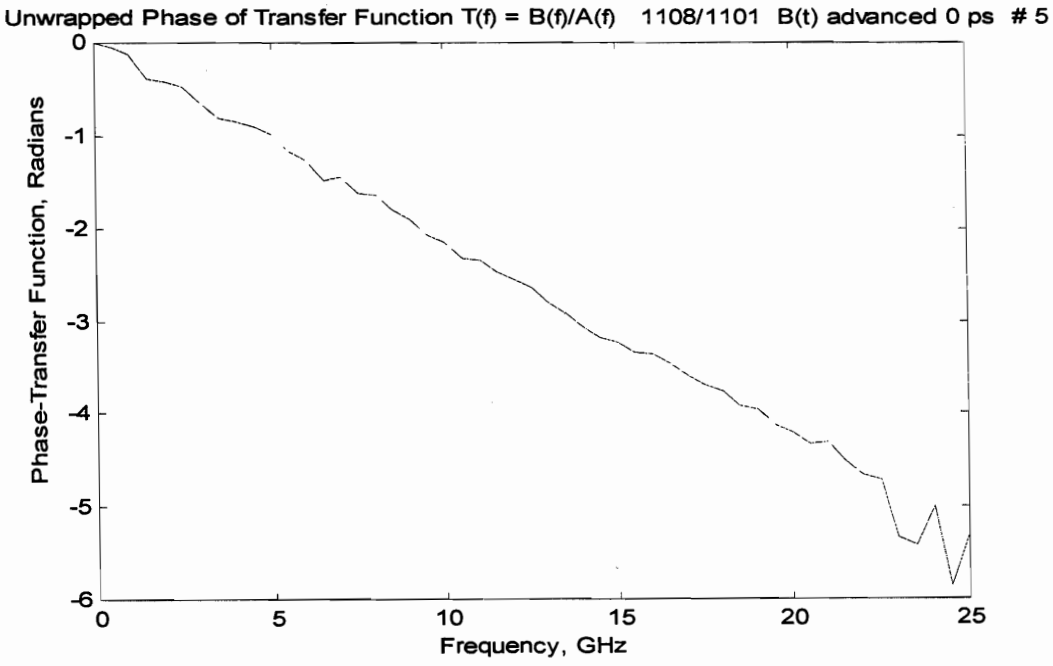

Figure 13. Phase of transfer function for propagation through differential length ($\ell_2 - \ell_1$) of type-236 artificial dielectric material between TEM-horn antennas

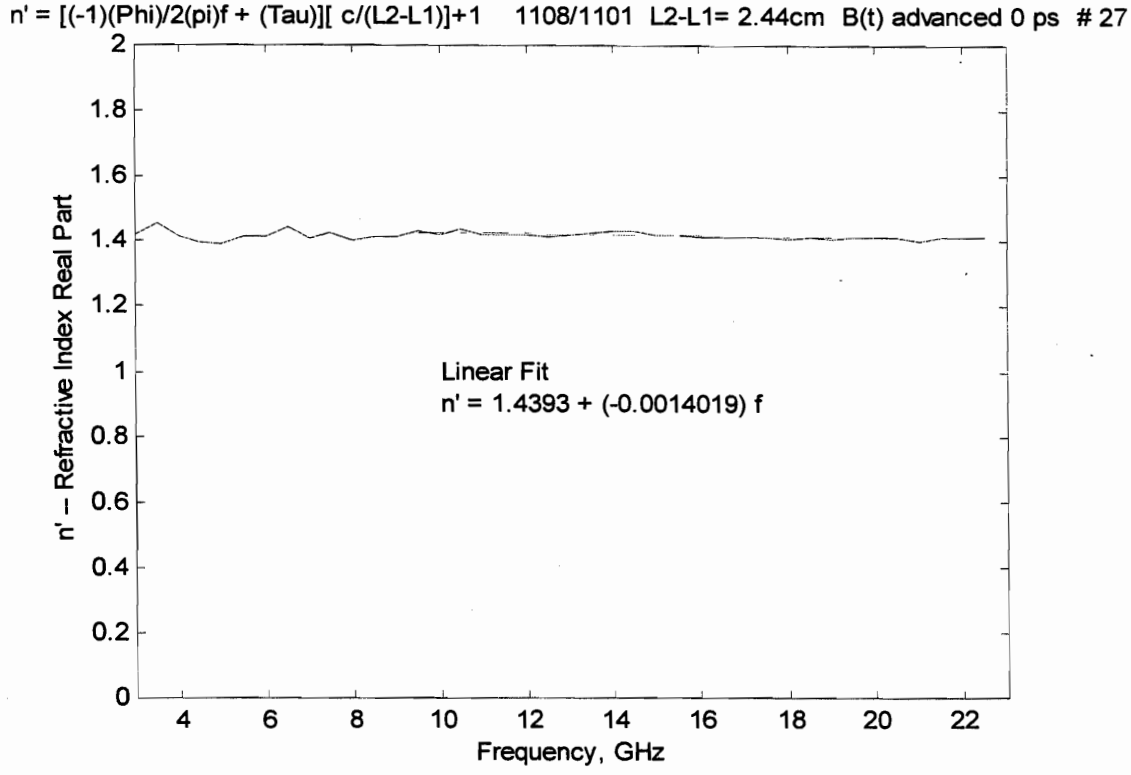

Figure 14. Real part of refractive index for type-236 artificial dielectric material calculated from time domain two antenna measurement

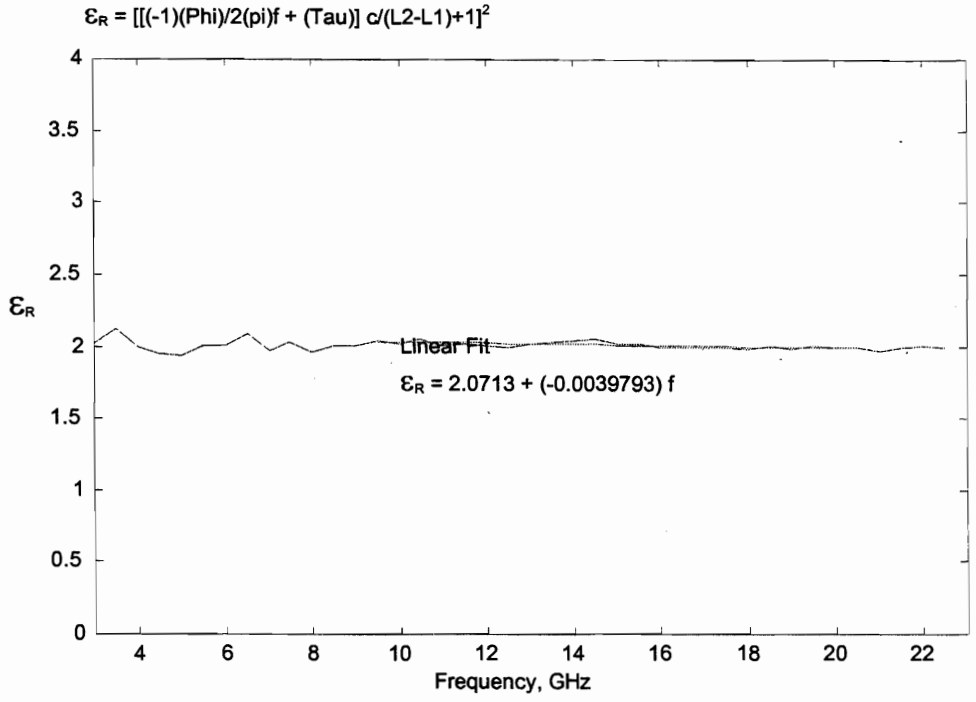

Figure 15. Relative permittivity for type-236 artificial dielectric material calculated from time domain two antenna measurement

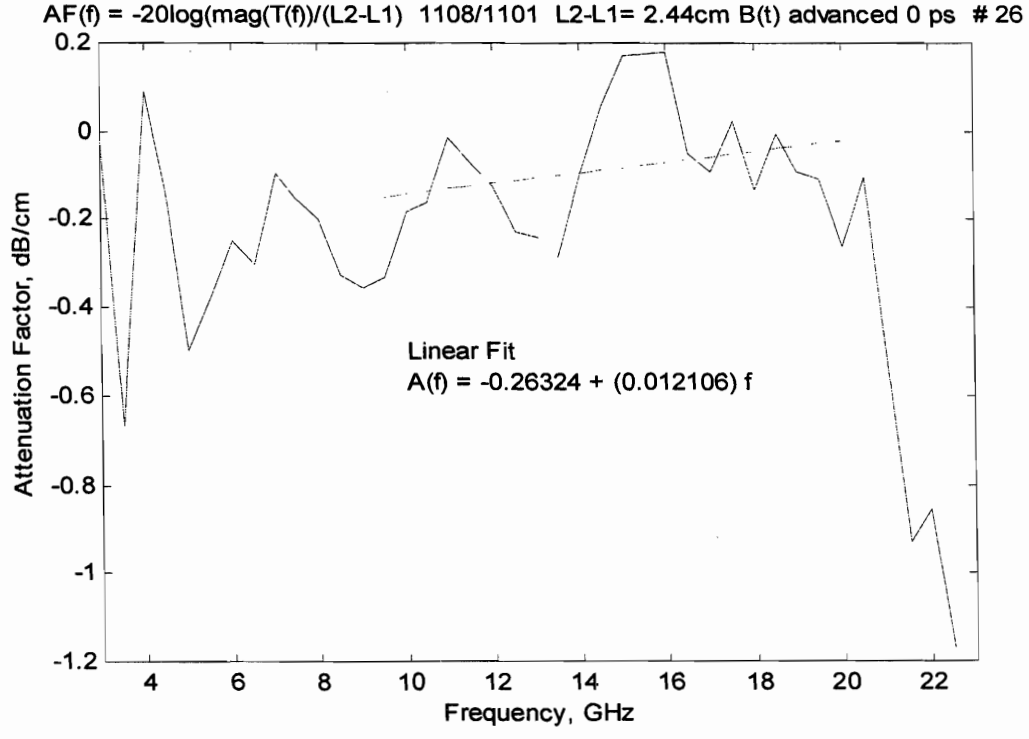

Figure 16. Attenuation factor for type-236 artificial dielectric material calculated from time domain two antenna measurement

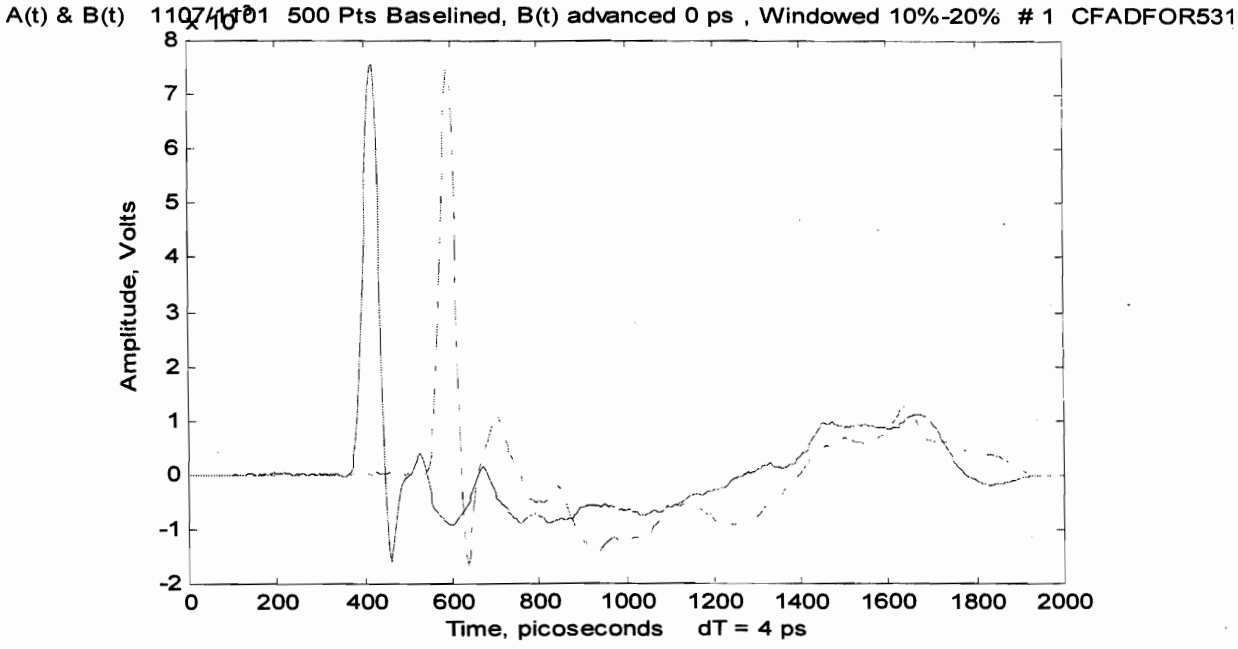

Figure 17. Time domain transmission waveforms A(t) and B(t) for propagation through lengths ℓ_1 and ℓ_2 of polyethylene between TEM-horn antennas

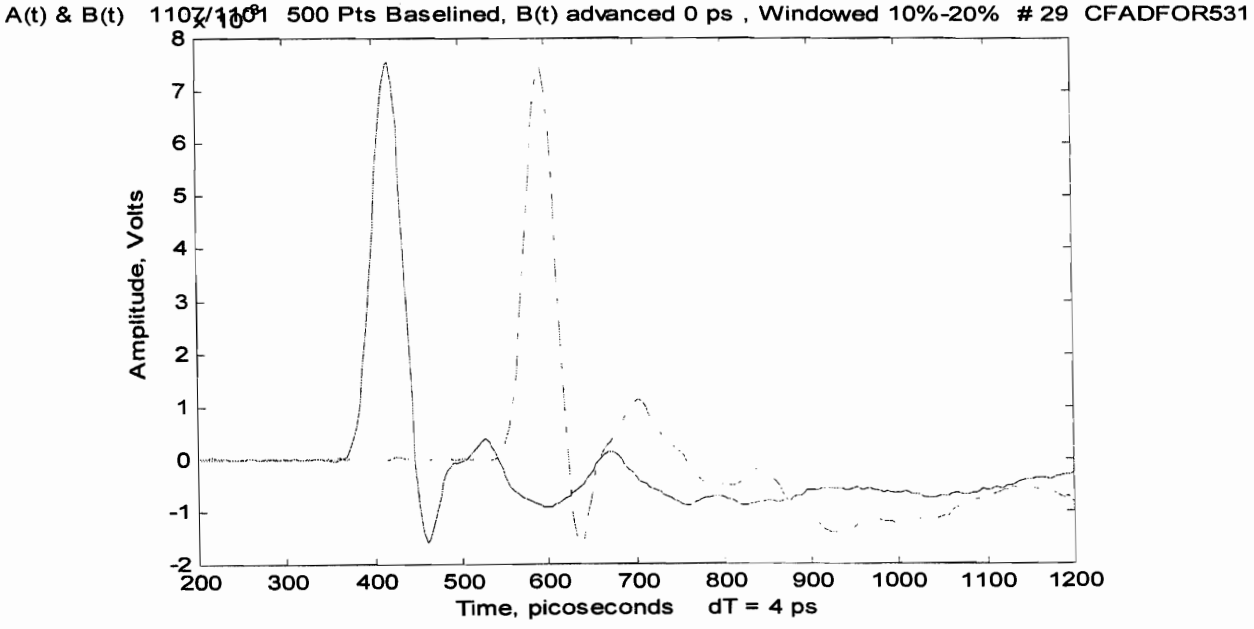

Figure 18. Time domain transmission waveforms A(t) and B(t) for propagation through lengths ℓ_1 and ℓ_2 of polyethylene between TEM-horn antennas at finer resolution

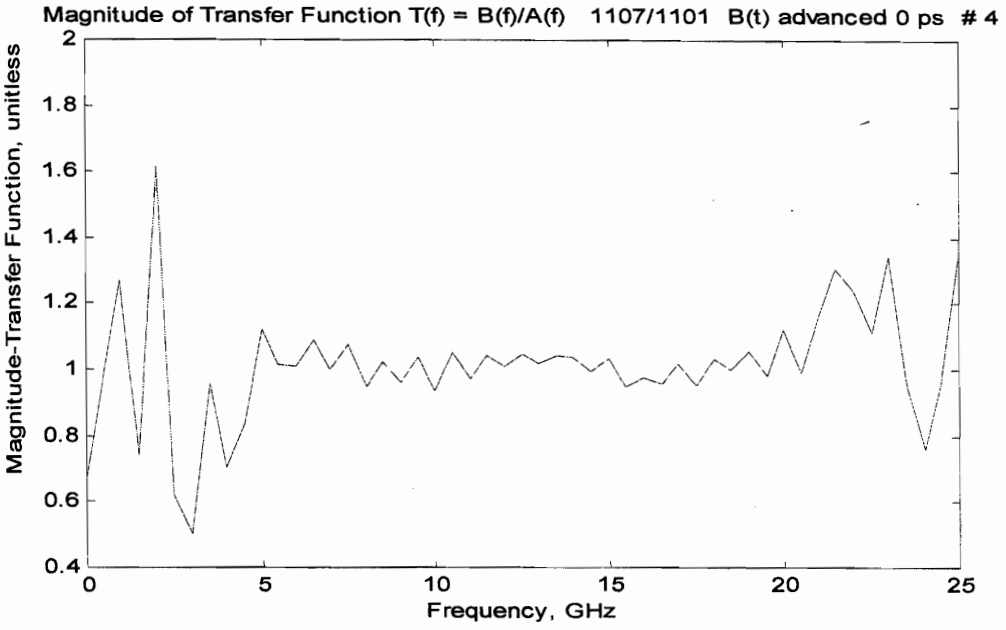

Figure 19. Magnitude of transfer function for propagation through differential length ($\ell_2 - \ell_1$) of polyethylene between TEM-horn antennas

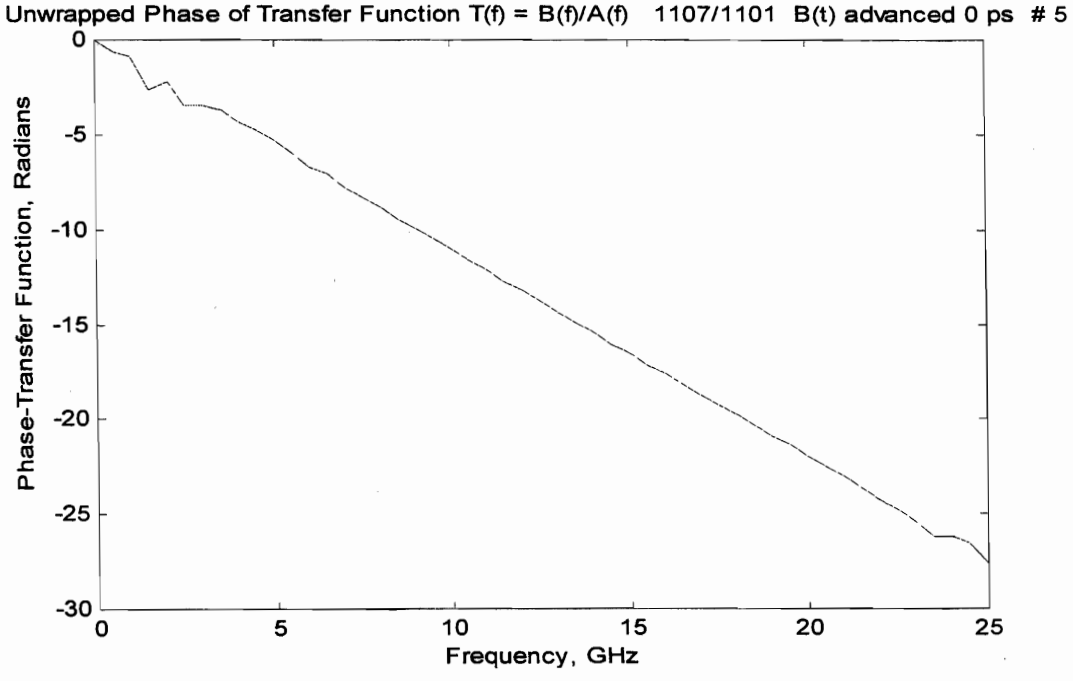

Figure 20. Phase of transfer function for propagation through differential length ($\ell_2 - \ell_1$) of polyethylene between TEM-horn antennas

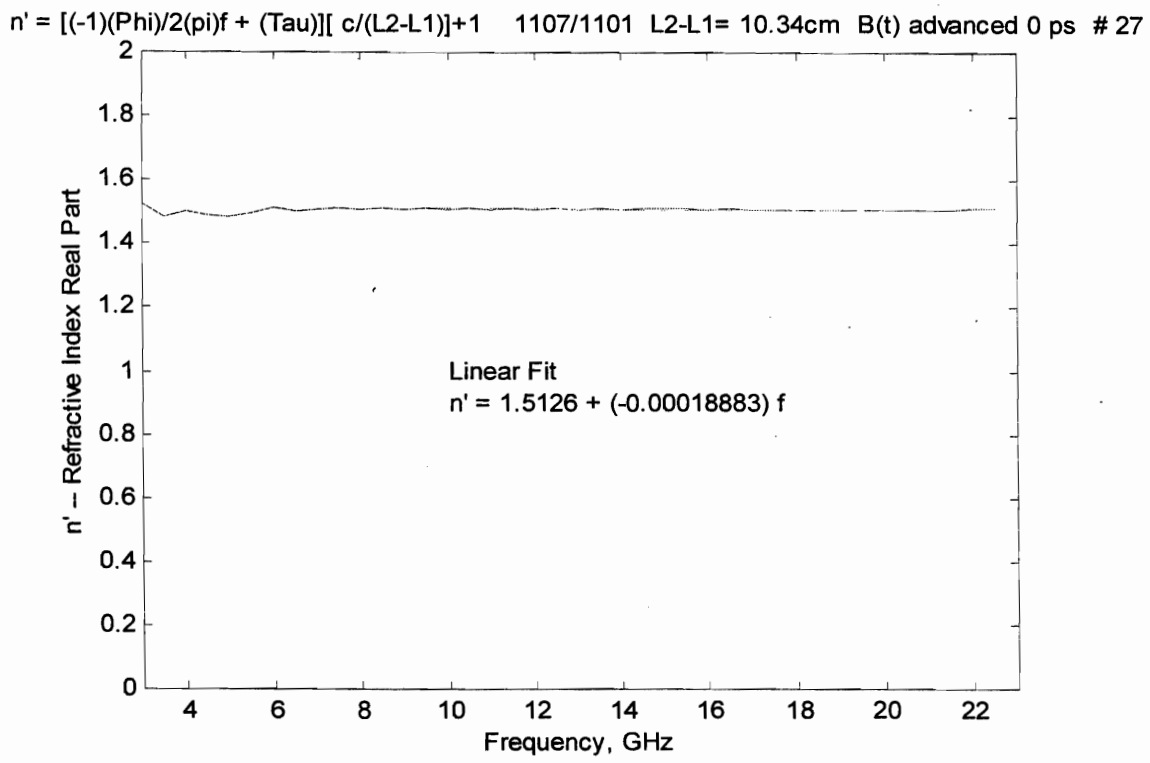

Figure 21. Real part of refractive index for polyethylene calculated from time domain two antenna measurement

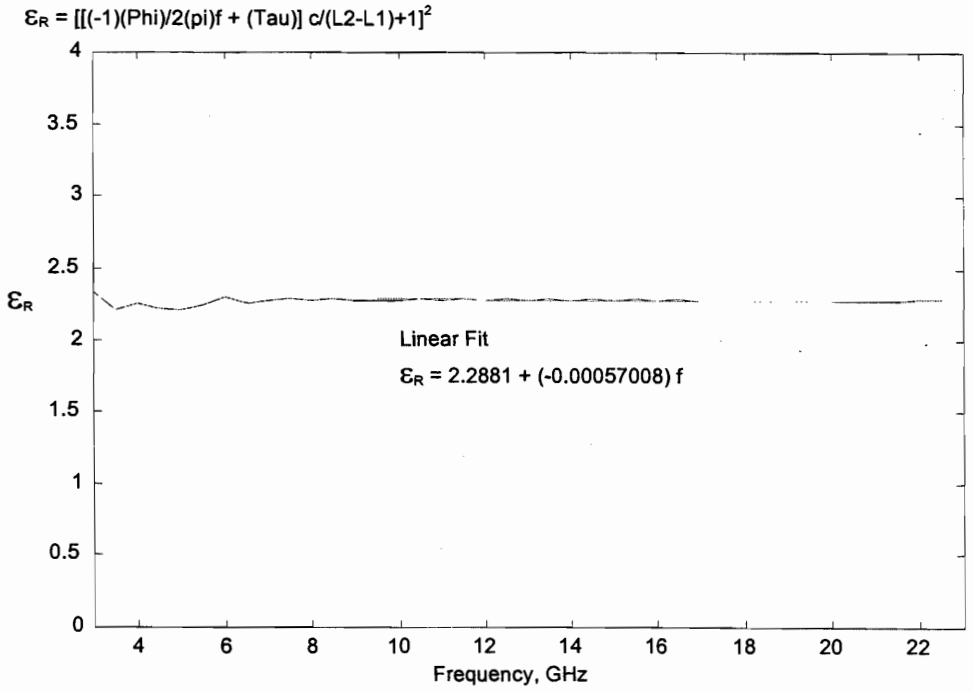

Figure 22. Relative permittivity for polyethylene calculated from time domain two antenna measurement

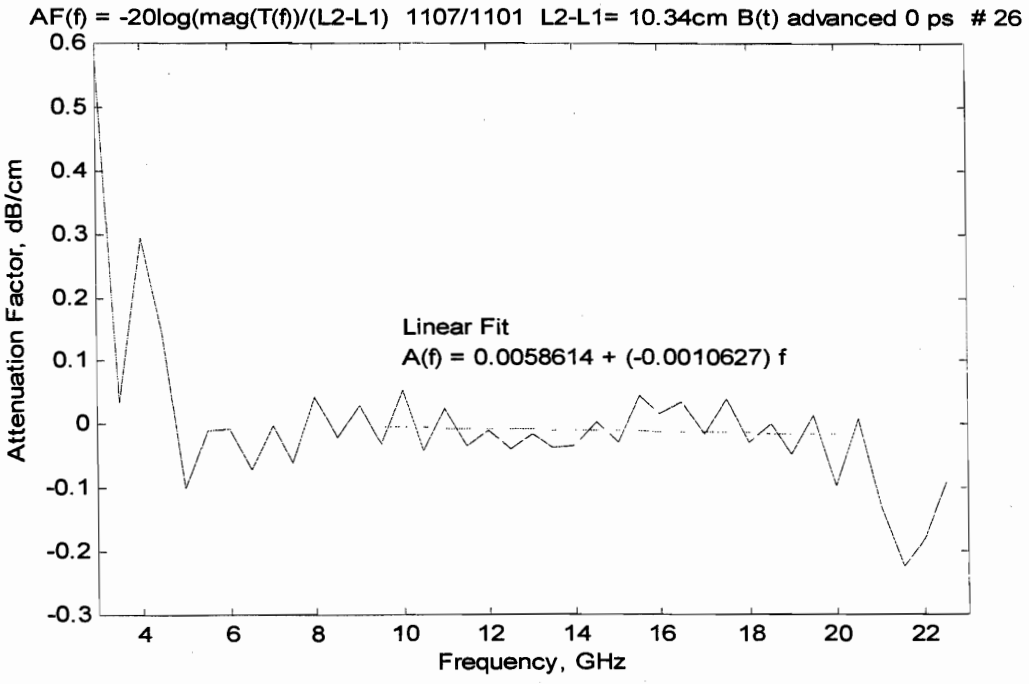

Figure 23. Attenuation factor for polyethylene calculated from time domain two antenna measurement

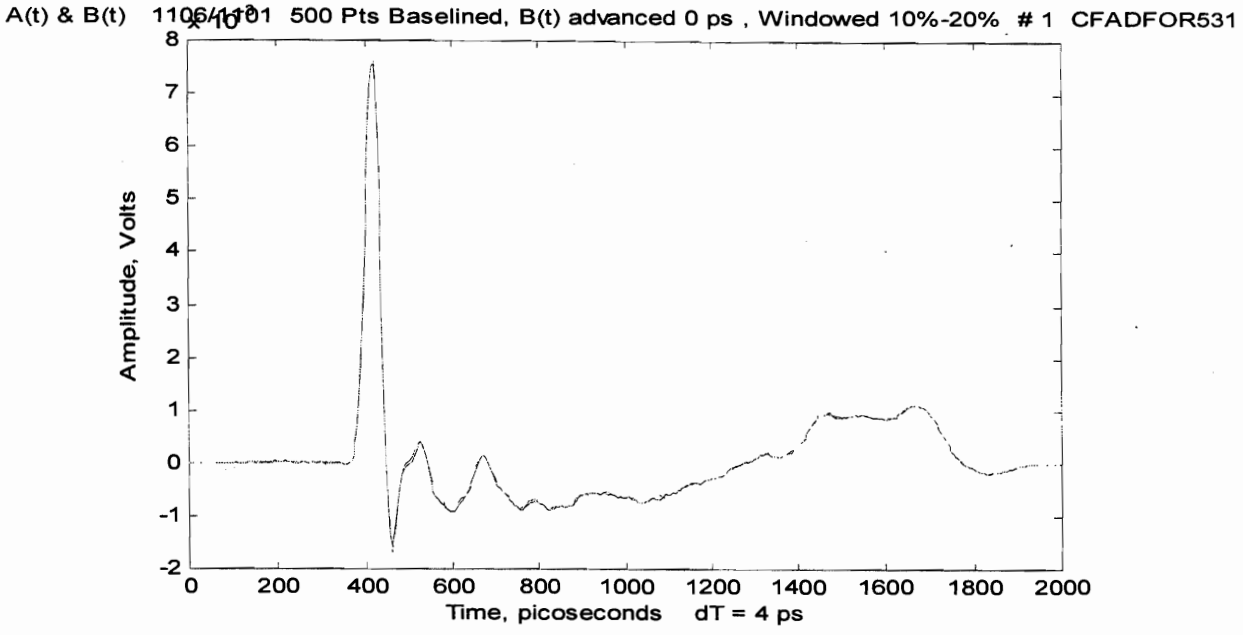

Figure 24. Time domain transmission waveforms A(t) and B(t) for propagation through lengths ℓ_1 and ℓ_2 of air between TEM-horn antennas

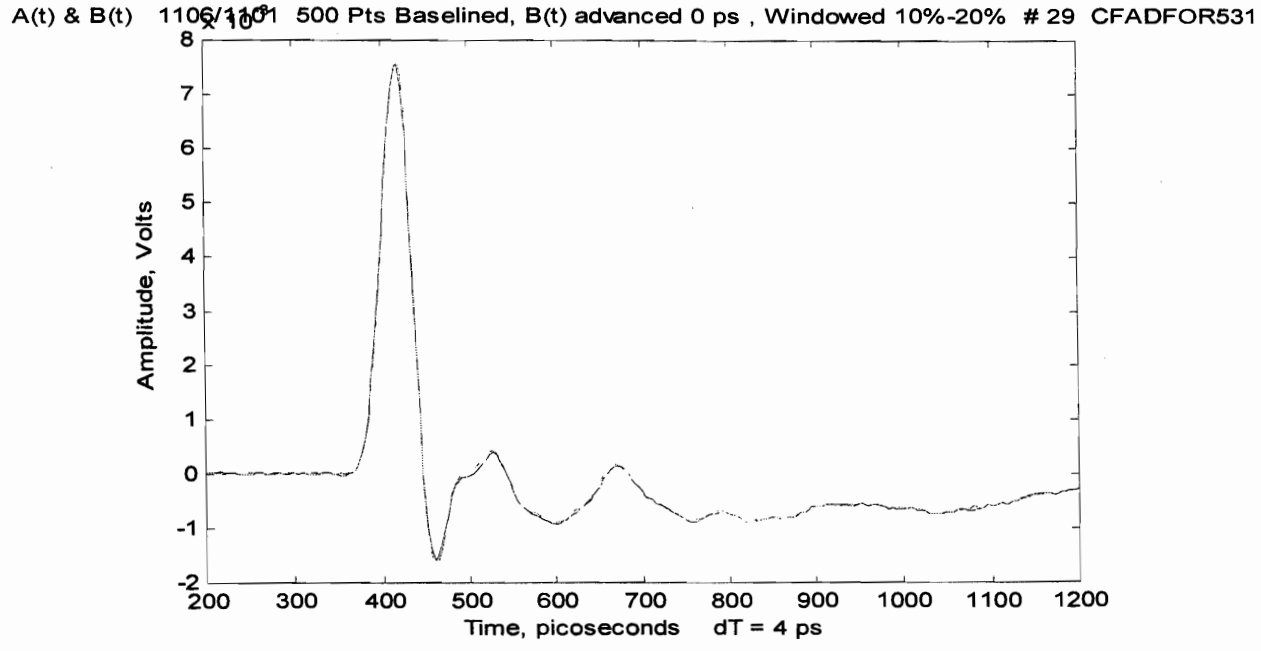

Figure 25. Time domain transmission waveforms A(t) and B(t) for propagation through lengths ℓ_1 and ℓ_2 of air between TEM-horn antennas at finer resolution

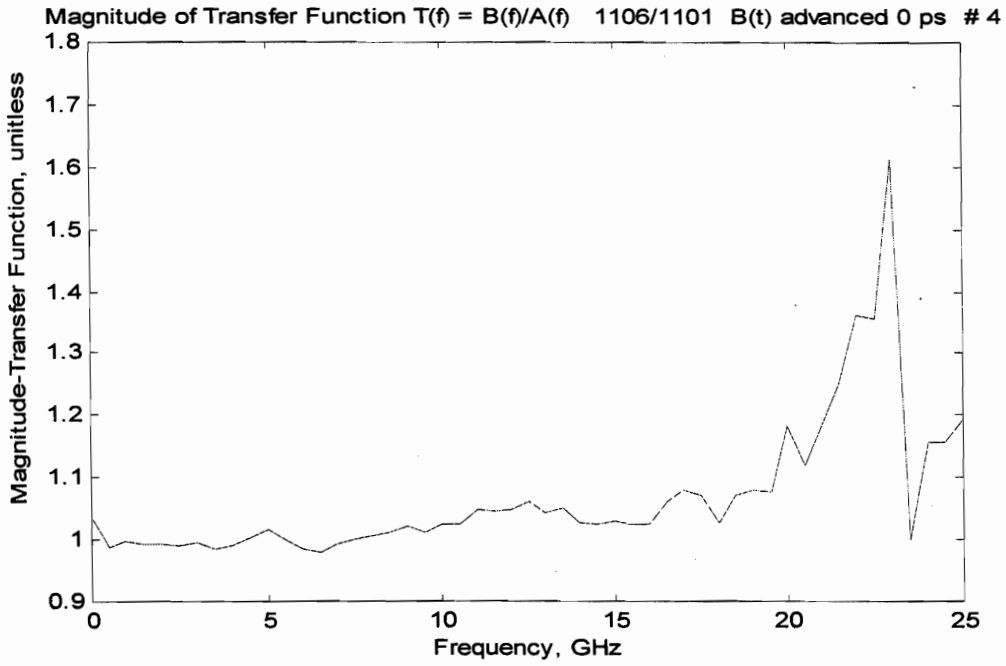

Figure 26. Magnitude of transfer function for propagation through differential length ($\ell_2 - \ell_1$) of air between TEM-horn antennas

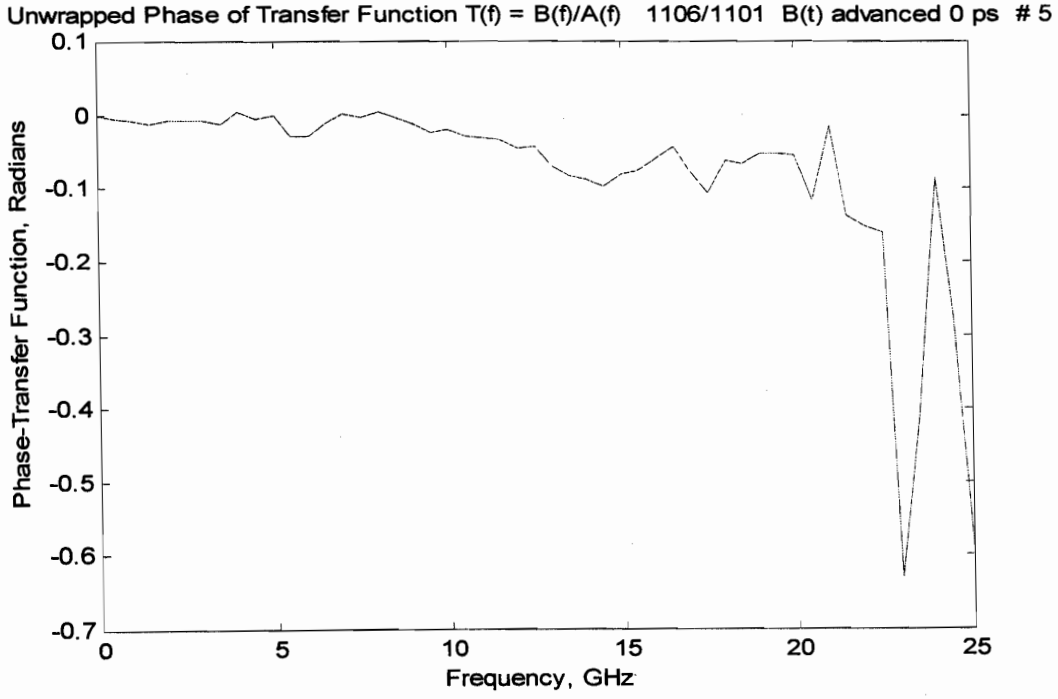

Figure 27. Phase of transfer function for propagation through differential length ($\ell_2 - \ell_1$) of air between TEM-horn antennas

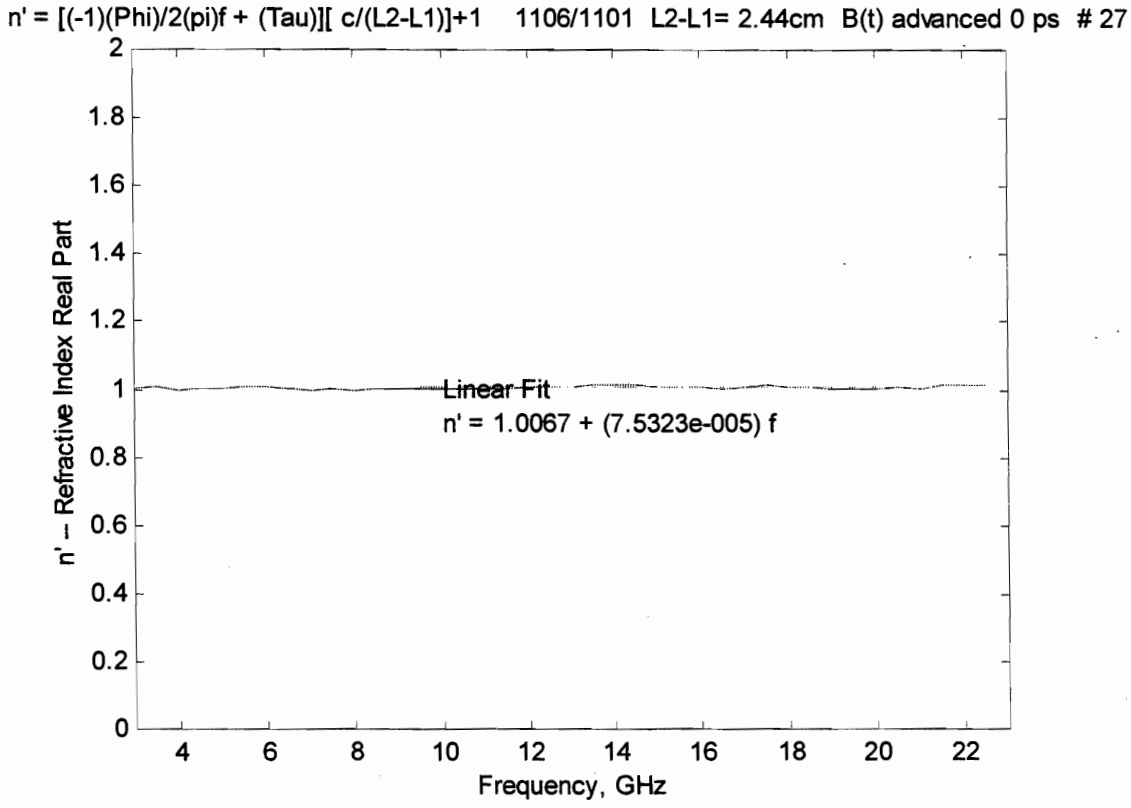

Figure 28. Real part of refractive index for air calculated from time domain two antenna measurement

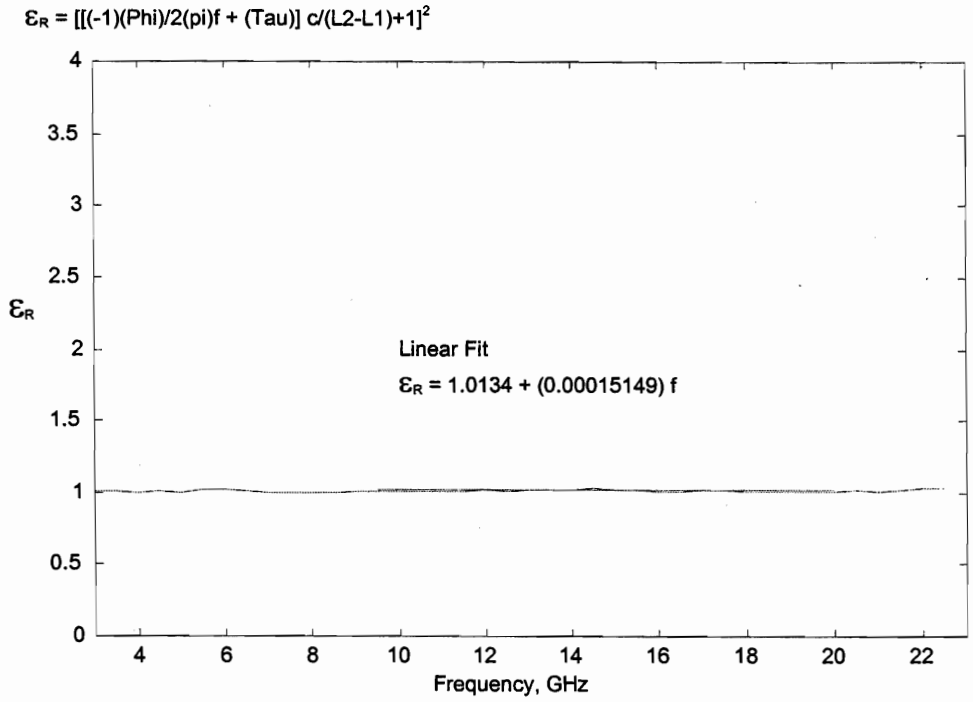

Figure 29. Relative permittivity for air calculated from time domain two antenna measurement

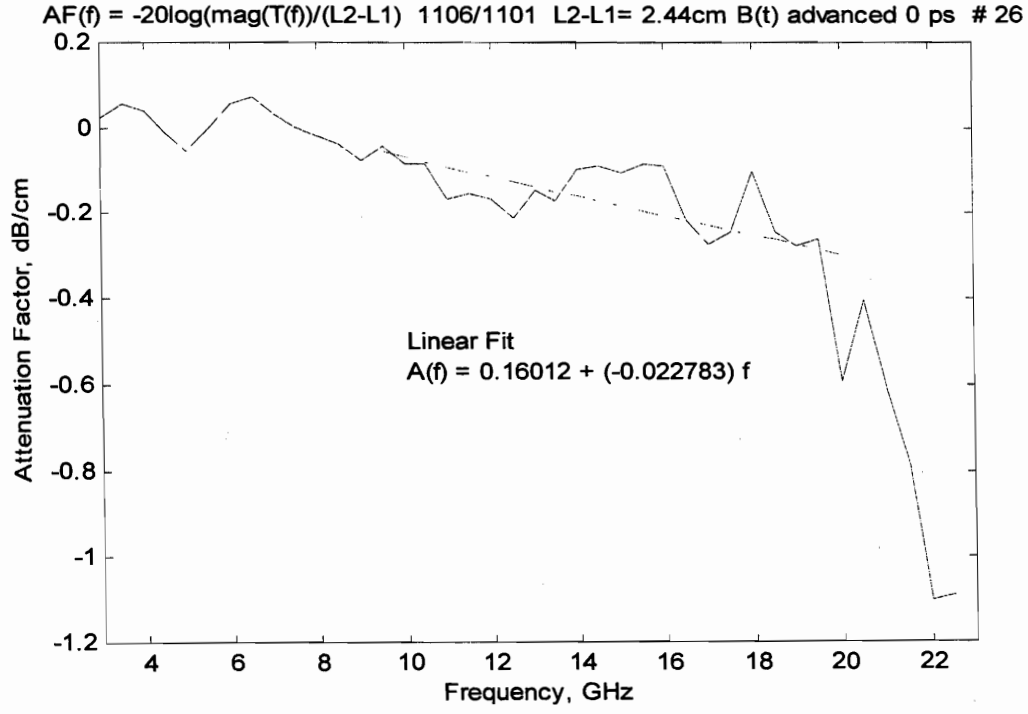

Figure 30. Attenuation factor for air calculated from time domain two antenna measurement

The refractive index n(f) is the key material dielectric property required to design a dielectric lens. For example, the dielectric lens of a IRA antenna can be directly designed using the same equations and techniques as for an optical lens if the refractive index is known. Table 3 summarizes the measured data on the refractive index for each of the materials studied by the two antenna transmission method. In each case, the value of n(f) is calculated for the discrete frequencies using the least squares linear fit equation which is given on the graph of the index for the material.

Table 3. Frequency Dependence of Refractive Index from Fourier Transformed Two Antenna Time Domain Radiated Wave Transmission Data

Real part of refractive index n = c/v as a function of frequency

Material	Frequency			
	2 GHz	5 GHz	10 GHz	20 GHz
type 265	1.66	1.66	1.65	1.64
type 236	1.44	1.43	1.42	1.41
polyethylene	1.51	1.51	1.51	1.51
Air	1.01	1.01	1.01	1.01

In order to quantify systematic errors of the measurement and to estimate accuracy, we performed two separate measurements with only air between the horn antennas. The measurements were taken one hour apart which is longer than the longest time period between any dielectric measurements. We arbitrarily choose a differential length ($\ell_2 - \ell_1$) of 2.44 cm for the calculations since this is the shortest length employed in any measurement of dielectric properties.

Figures 24 through 30 show the resulting data set for this calibration for system background noise level. The time of the two peaks on figure 25 line up to within 1 ps giving a time domain calculation of refractive index and permittivity which are both exactly 1.00. The transfer function of figure 27 is flat at 1.0, and the phase error is under 0.05 radian up to 10 GHz. Slightly higher errors are seen in the range of 10 to 20 GHz. The data of figures 28 and 29 show that the refractive index and relative permittivity are flat with mean values of 1.007 and 1.014 over the range of 3 to 23 GHz. The attenuation factor has an intercept value of 0.16 db/cm rather than 0.00. We can normalize AF(f) against this systematic error by shifting the intercept to zero.

From the background calibration, we infer that the two antenna measurement technique is highly accurate in determining permittivity and index of refraction with error bars at the 1% level but is less accurate at determining attenuation factors for low loss materials. The lower limit on accurate attenuation factors is approximately 0.2 db/cm. The observed system background level for attenuation measurements corresponds to slight drifts at the fractional decibel level in the output voltage of the pulse generator or sampler sensitivity. These variations could occur as a result of temperature shifts or other system drift with time. The sensitivity of the measurement appears to be sufficient to identify any problems with high loss materials but is inadequate to accurately quantify the attenuation factor for very low loss materials such as teflon.

Additional inaccuracy can occur in the two antenna radiated wave measurement method due to waves which diffract around the edges of the sample. This problem does not occur in the theory which assumes samples of infinite transverse extent. In the laboratory measurement, the physical samples are of finite size, and we must minimize diffraction at the edges. The diffraction can be reduced by placing the samples near one of the antennas, but this is a region where significant wave front curvature occurs. The theory assumes plane wave propagation. The positioning of the sample is, thus, a compromise between signal leakage and wave curvature. For the large (18 inch X 18 inch) polyethylene sample diffraction was not a problem, and we could place the sample far from the antenna. For the other materials we had smaller samples, and it was necessary to place the samples near the antenna where wave curvature was significant. This could effect the accuracy of the measurement, but the magnitude of the error is hard to quantify.

One goal of the measurement was to compare dielectric properties of the type 265 artificial dielectric material for waves traveling parallel or perpendicular to a preferred propagation axis. The manufacturer supplied the type 265 material as flat plates which were 12 inch X 12 inch X 1 inch thick. The material was intended to be used with propagation through the face, and performance was unknown for transverse propagation. In order to measure propagation transverse to the preferred axis, it would be necessary to cut apart the samples and reconfigure them as a stack of 12 slabs, where each slab had dimensions of 1 inch X 12 inches. This would yield a 12 inch X 12 inch X 1 inch sample suitable for wave propagation through the material transverse to the preferred access. Such fabrication would be possible but difficult. Uniformity could also be compromised by the adhesive used to bond the pieces together.

As an alternative to fabricating the complex samples, we developed a new transmission line test fixture which could be used for small samples. This allowed us to cut reasonable sized samples of the type 265 material to compare propagation of waves traveling parallel and perpendicular to the preferred axis. In addition, this approach avoided the problem of diffraction at the edge of the sample. The mathematical analysis and data processing for the transmission line fixture was identical to that used for the freely propagating wave data. The next section will describe the test fixture in more detail and present propagation data obtained for the artificial dielectric materials using the bounded wave technique.

4. MEASUREMENTS OF COMPLEX DIELECTRIC PROPERTIES USING THE BOUNDED WAVE TEM CELL TEST FIXTURE

In this section we describe the TEM cell test fixture and the data on material dielectric properties which were determined using it. The transmission line test fixture was developed in order to allow small rectangular dielectric samples to be measured with propagation parallel to and perpendicular to a preferred propagation axis. This was not feasible with the two antenna measurement approach. The bounded wave transmission line measurement also avoided the difficulties of edge diffraction which were found to be a problem with the two antenna method. We have performed previous measurements [1,7] in a coaxial transmission line test fixture, but the coaxial test fixture was not compatible with the measurement of propagation in the perpendicular orientation using the samples available to us. For this reason, we designed and fabricated a new TEM cell specifically for this measurement.

The TEM cell was an open air dielectric strip line section above ground-plane with transition sections at both ends. The rectangular samples could be inserted into the strip line from the side. Figure 31 is a diagram showing a side view of the TEM cell, while figures 32 through 34 are photographs showing details of the construction. The line was designed to have a 50 ohm impedance in the unloaded test section to minimize multiple reflections from the discontinuity at the sample. The upper conductor was constructed of 10 mil brass sheet while the ground plane consisted of a 6.5 inch X 12 inch copper clad circuit board. The wave was launched and received at the apex of the triangular transition sections by a direct attachment of the brass sheet to the center conductor of a miniature (0.085 inch diameter) semirigid coaxial cable. The upper conductor was supported by hollow polystyrene spacers which gave minimal perturbation to the traveling wave. The test section had a length of 10.2 cm and a width of 4.75 cm. The transition sections each had a length of 7.11 cm.

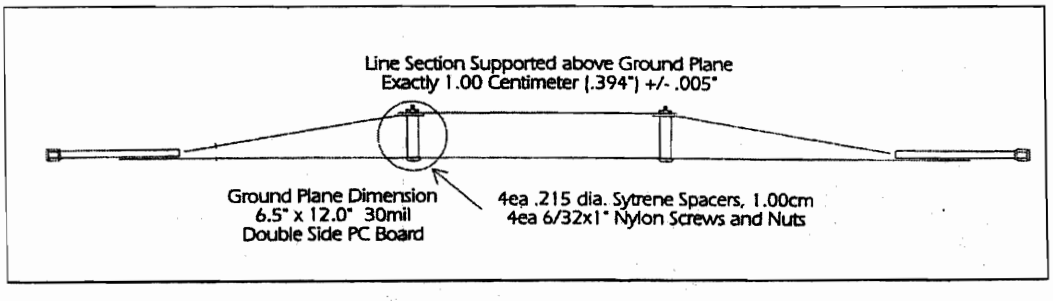

Figure 31. Side view of TEM-cell

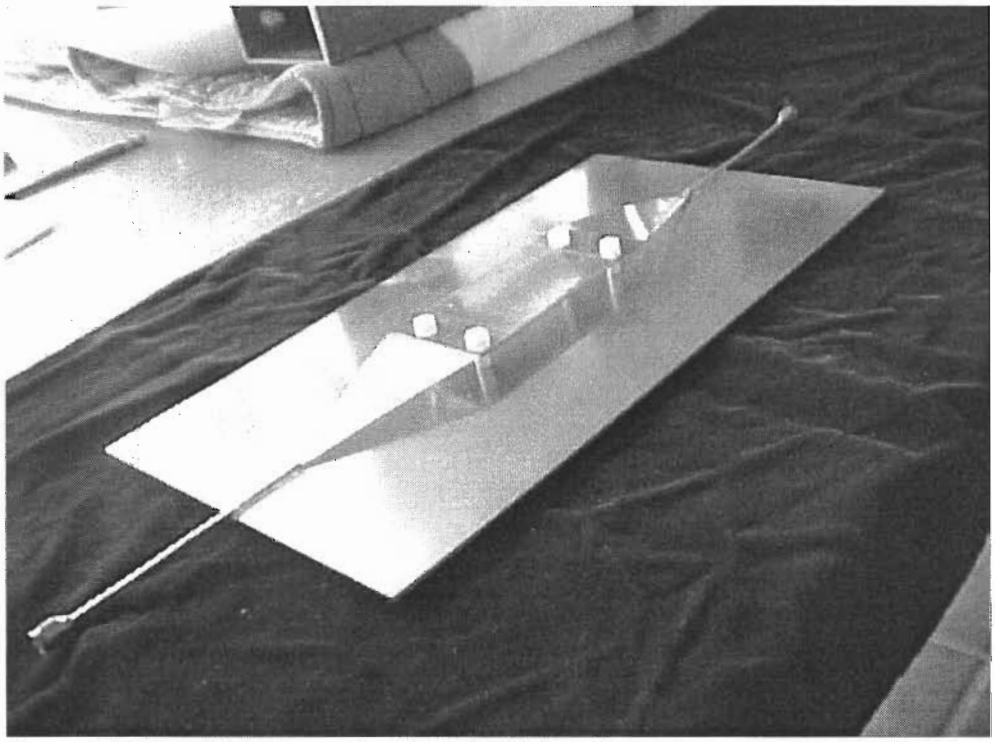

Figure 32. Photograph of the TEM-cell

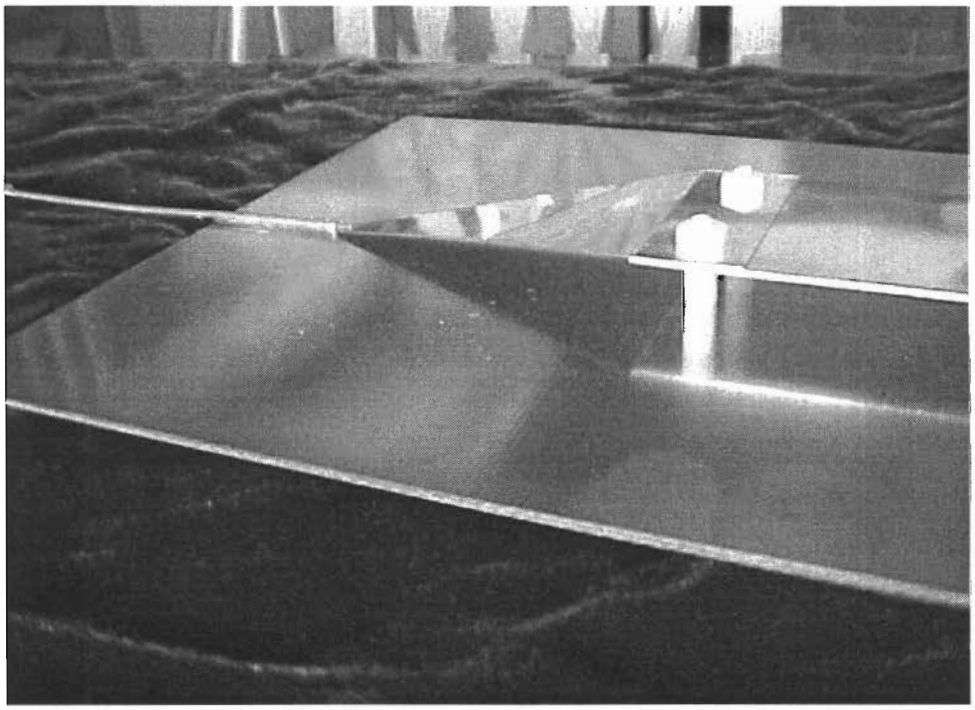

Figure 33. Transition from coaxial cable to parallel plate above ground

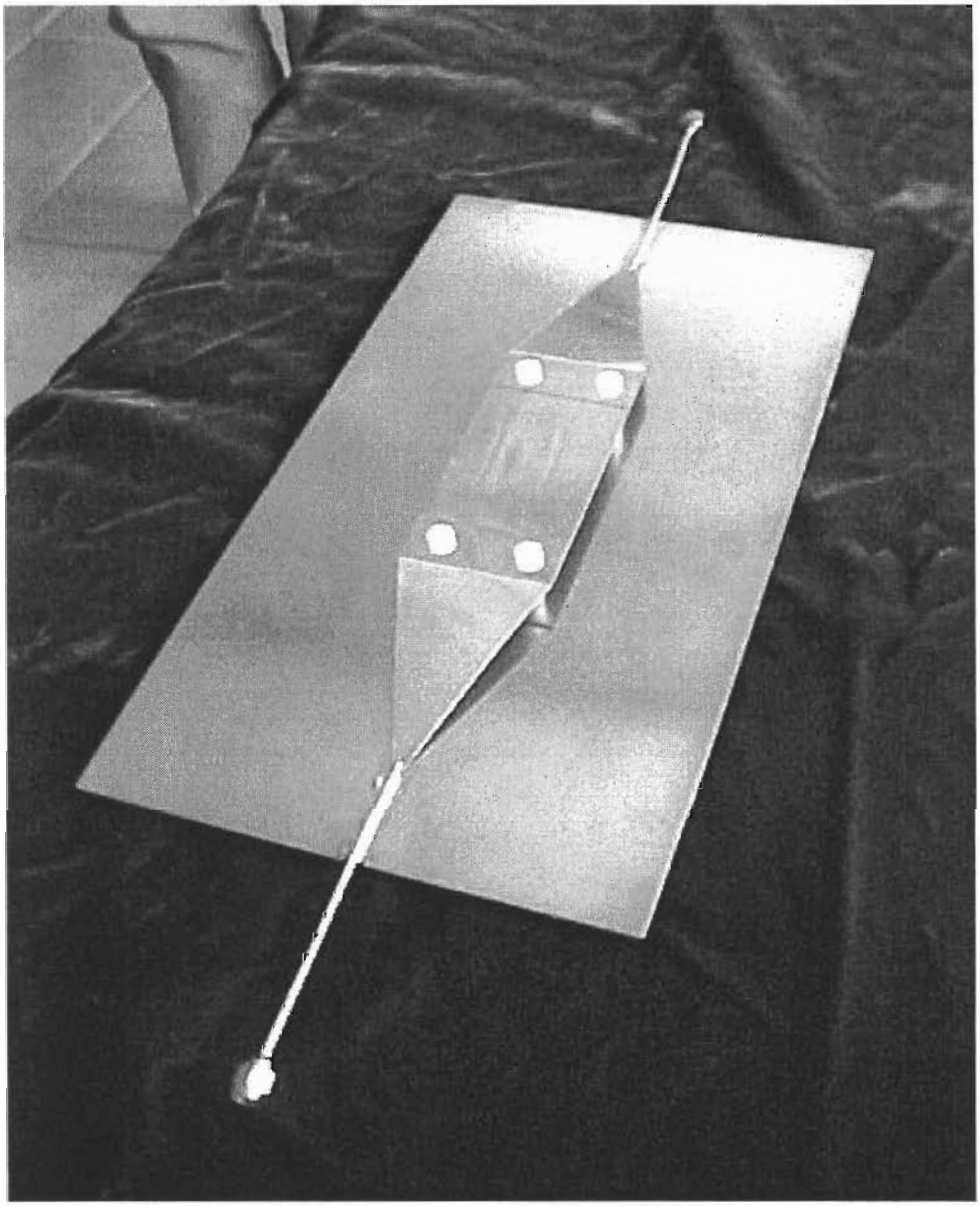

Figure 34. Photograph of the TEM-cell viewed from above

The electrical performance of the TEM cell was characterized by transmission measurement and TDR measurements using the Tektronix 11801 sampling oscilloscope. TDR measurements showed a transmission line impedance of 51 ohms in the straight section and 55 ohms in the transistions. The TEM cell was capable of providing a transmitted derivative impulse with a width of 35 ps (FWHM). This included the response of the TEM cell, pulse generator, sampling head, and cabling of the system. These measurements confirm proper operation of the TEM cell.

Rectangular samples were prepared for insertion in the TEM-cell bounded wave transmission line test fixture. Samples of the type 265 and type 236 artificial dielectric material and the polyethylene reference material were machined. Each sample had dimensions of 1.000 cm X 1.000 cm X 10 cm. The samples were inspected by optical metrology instruments and confirmed to have an accuracy better than 0.002 cm along each of the critical 1 cm dimensions.

The measurement technique was as described in section 2 for use with the two-antenna method. The pulse generator provided a fast risetime step function waveform which was differentiated to give the impulse wave shape used for the transmission measurement. The transmitted voltage waveform was recorded with the Tektronix 11801 sampling digitizer, and the total system response in measurement mode was less than 35 ps. For each measurement the shorter of the two samples had a length ℓ_1 of 1.000 cm, while the longer sample had a length ℓ_2 of 5.00 cm. The differential material length ($\ell_2 - \ell_1$) was thus 4.00 $\pm$0.01 cm for each measurement reported in this section. The analysis method employed to convert the time domain waveforms to frequency domain dielectric properties was exactly as described in section 3 except that the sampling point spacing was increased to give a total time window of 10 ns.

We begin with analysis of the TEM-cell data collected with the type 265 artificial dielectric oriented for propagation in the preferred direction as specified by the material manufacturer. We label this data set as type 265 $\|$ material data. Figure 35 shows the time domain data resulting from propagating the radiated pulse through two different lengths of the material. The first pulse in time (waveform A(t)) has propagated through the shorter sample. The second pulse has propagated through the longer sample. The differential path length through the material ($\ell_2 - \ell_1$) was 4.00 cm. Both waveforms show a narrow transmitted impulse. The later waveform is broadened and slightly reduced in amplitude due to the passage through the additional length ($\ell_2 - \ell_1$) of material.

Figure 36 shows the time domain data at a finer time resolution. The measured time delay Δt between the two peaks is 64 ps. Equation (7) gives a value of 1.48 for the refractive index (n) calculated directly from the time domain data. The relative permittivity calculated as the square of n is 2.19 for the type 265 || material. The time domain calculation gives a single number corresponding to the mean value over the frequency range contained in the exciting pulse. To get the frequency dependence of n, we window the time sequence and Fourier transform into the frequency domain.

Figures 37 and 38 show the magnitude and unwrapped phase of the computed transfer function T(f). The phase is approximately linear. Close examination of figure 38 indicates slight deviation from linear phase which is the result of dispersion due to frequency dependent wave speed. The magnitude is well behaved over the range of 3 to 23 GHz showing a uniform falloff from unity with increasing frequency.

Figure 39 shows the real part of the refractive index which is calculated from the unwrapped phase data using equation (5). The data is plotted as a function of frequency over the range of 3 to 23 GHz. The refractive index is nearly constant with frequency with a mean value of 1.48 which matches the value obtained from time domain calculation using equation (7). A least squares linear fit to the data is plotted in figure 39, and the slope and intercept values are displayed on the figure. There is a slight decrease in n'(f) with increasing frequency.

Figure 40 plots the relative permittivity $\varepsilon_R(f) = \frac{\varepsilon(f)}{\varepsilon_o}$ which is calculated as the square of the refractive index. The straight line fit through the data points is also plotted on the figure. The relative permittivity has a mean value of 2.20 with a slight decrease in value with increasing frequency. Figure 41 shows the attenuation factor AF(f) which is calculated from the magnitude data using equation (6). The attenuation factor in decibels per unit length increases with frequency. The straight line fit indicates a value of 0.4 db/cm at 10 GHz.

The same technique was applied to characterize the type 265 artificial dielectric material for propagation perpendicular to the preferred propagation direction specified by the manufacturer. We label this data set as type 265 $\perp$ material data. Figures 41 through 47 show the corresponding data sets for the type 265 $\perp$ material. Visually the graphs all appear identical to the graphs of figures 35 through 41 for the type 265 || material. A time shift Δt of 63 ps was measured between the two waveforms giving values of 1.47 and 2.17 for the refractive index and relative permittivity using

equation (7). The frequency domain calculation of refractive index gives a mean value of 1.48, while the frequency domain calculation of relative permittivity gives a mean value of 2.19. The attenuation factor increases with frequency to a value of 0.4 db/cm at 10 GHz. All of the measured parameters are identical to those for the type 265 || material within the measurement accuracy of the apparatus. That is, we see no measureable difference in the material dielectric properties for waves propagating along or transverse to the manufacturers specifiied propagation axis. The type 265 artificial dielectric material appears to be isotropic.

The type 236 artificial dielectric material sample with a differential sample length ($\ell_2 - \ell_1$) of 4.00 cm was characterized in the same way. Figures 49 through 55 show the resulting data set for the type 236 material. The time shift measured from figure 50 was 54 ps which gives a value of 1.41 for the refractive index through equation 7. A value of 1.97 is calculated for the relative permittivity. Figures 51 and 52 show a well behaved transfer function T(f) with a magnitude near unity and linear phase delay with frequency over the range of 3 to 23 GHz. Figures 53 and 54 show that the refractive index and relative permittivity are almost independent of frequency with mean values of 1.40 and 1.95 which match the time domain calculations. Figure 55 shows that the attenuation coefficient per unit length increases with frequency.

Figures 56 through 62 show the corresponding data set for the polyethylene reference material again using a differential sample length ($\ell_2 - \ell_1$) of 4.00 cm. The time domain data of figure 57 shows a time delay of 68 ps between the two peaks which gives a refractive index of 1.51 and relative permittivity of 2.28.

The transfer function T(f) shows a highly linear phase (see figure 58) and a magnitude near unity (see figure 59). The refractive index shown by figure 60 is flat with frequency having a mean value of 1.50, while the relative permittivity shown by figure 61 is also flat with frequency with a mean value of 2.28. These values exactly match the values calculated directly from the time domain data and are in excellent agreement with the published values of [3]. The close agreement of the measured values of the dielectric properties to the published values validates the technique.

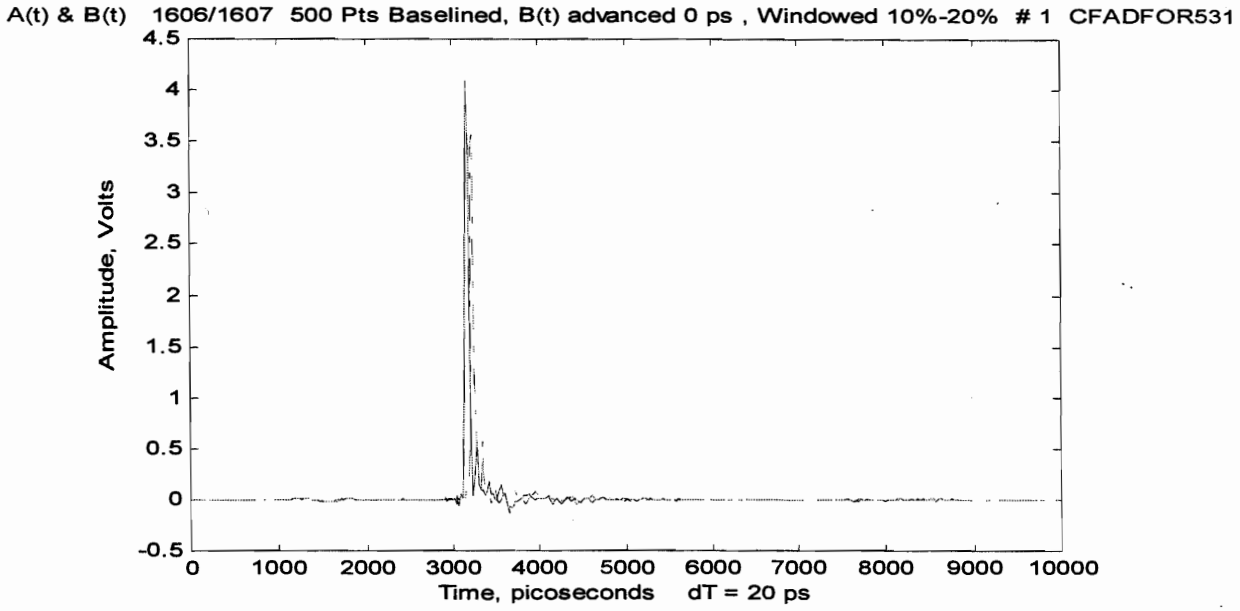

Figure 35. Time domain transmission waveforms A(t) and B(t) for propagation through lengths ℓ_1 and ℓ_2 of type-265 || artificial dielectric material in TEM-cell

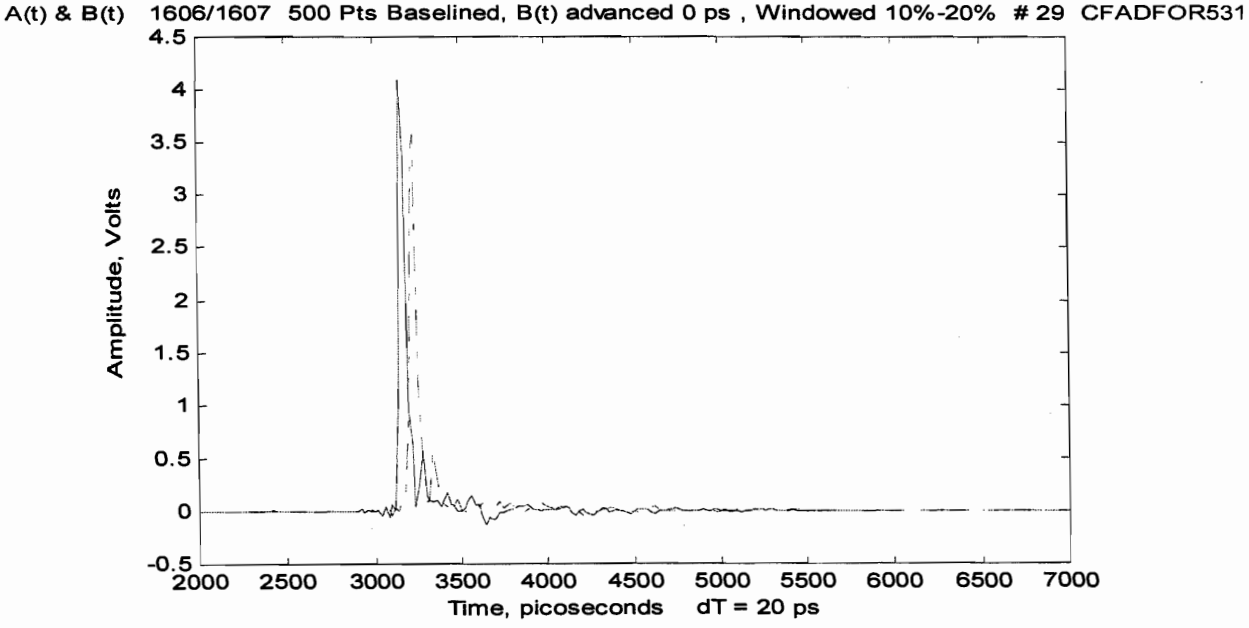

Figure 36. Time domain transmission waveforms A(t) and B(t) for propagation through lengths ℓ_1 and ℓ_2 of type-265 || artificial dielectric material in TEM-cell at finer resolution

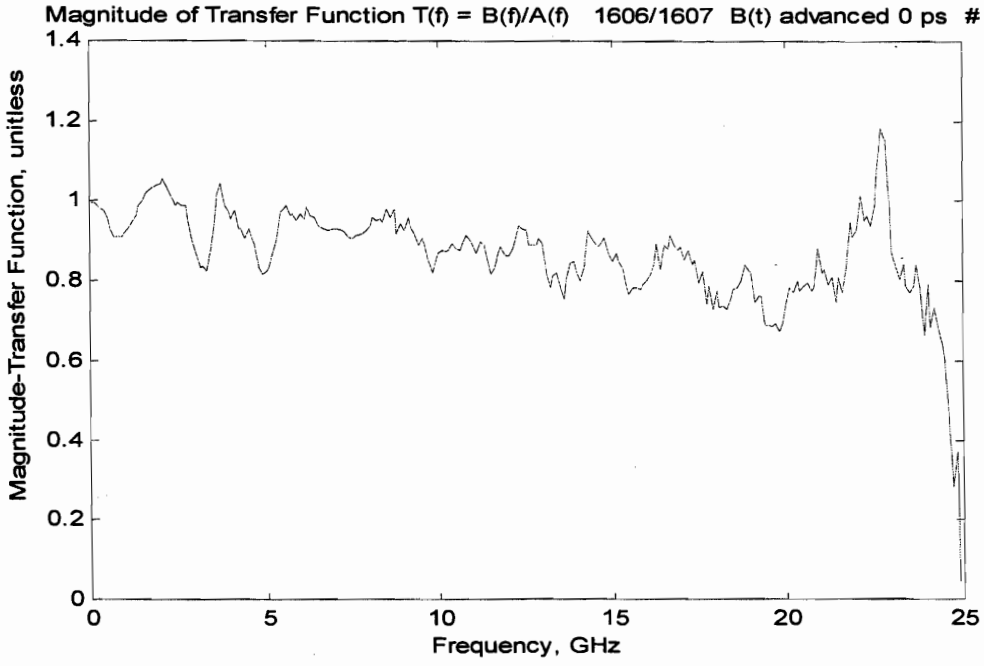

Figure 37. Magnitude of transfer function for propagation through differential length ($\ell_2 - \ell_1$) of type-265 || artificial dielectric material in TEM-cell

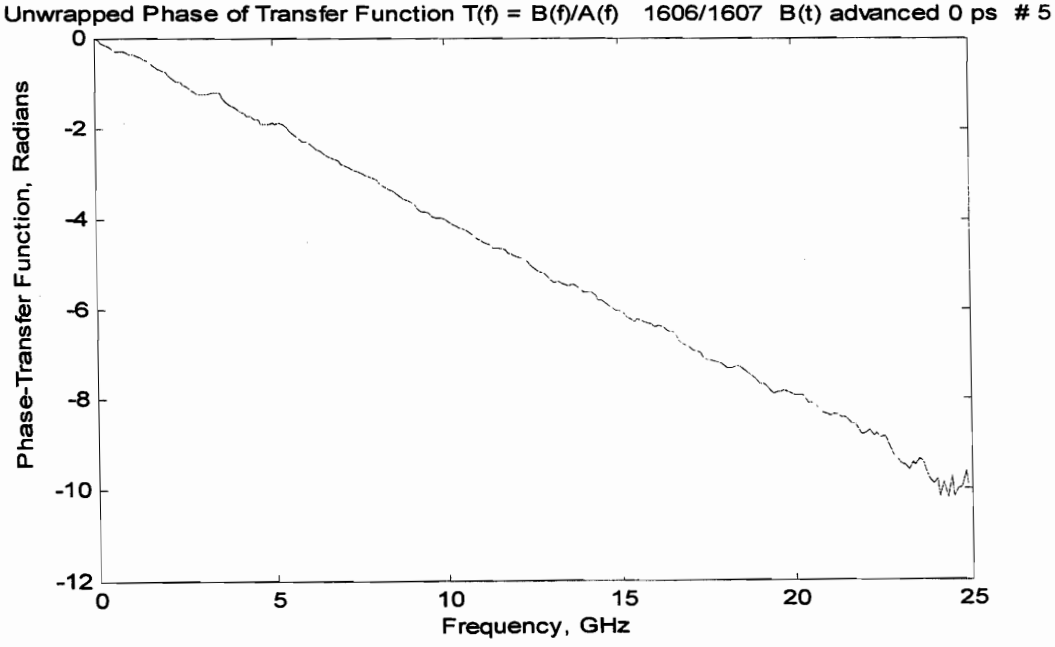

Figure 38. Phase of transfer function for propagation through differential length ($\ell_2 - \ell_1$) of type-265 || artificial dielectric material in TEM-cell

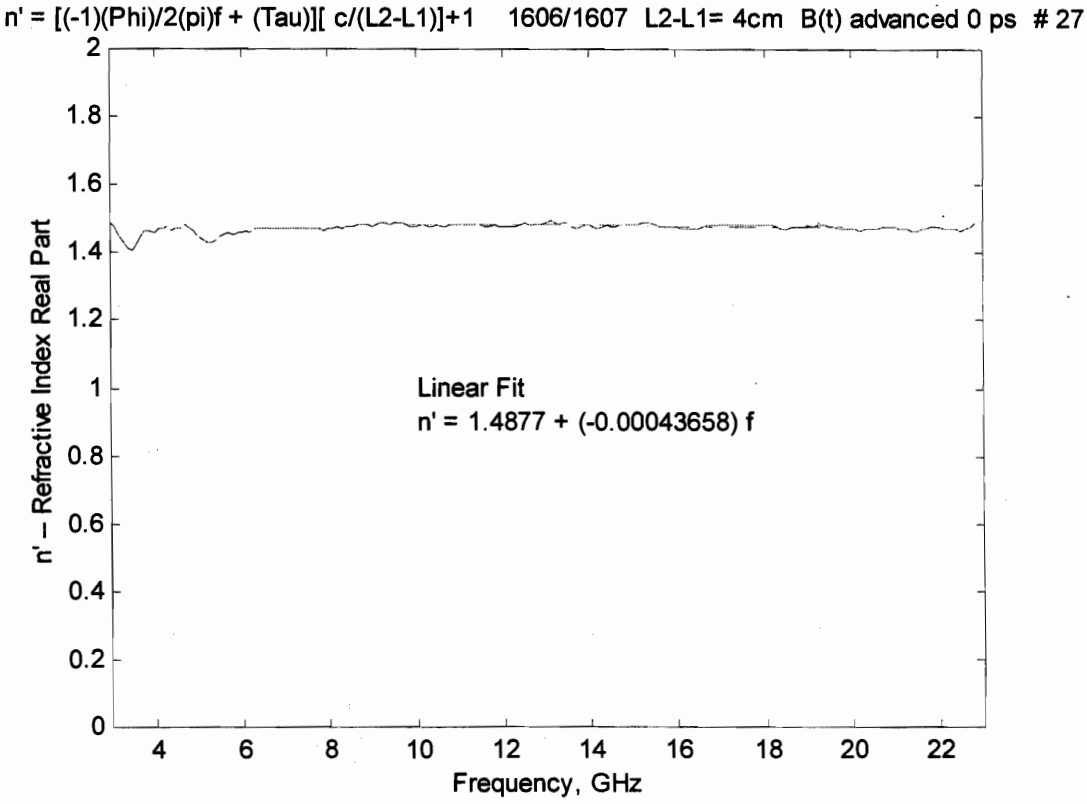

Figure 39. Real part of refractive index for type-265 || artificial dielectric material calculated from time domain TEM-cell measurement

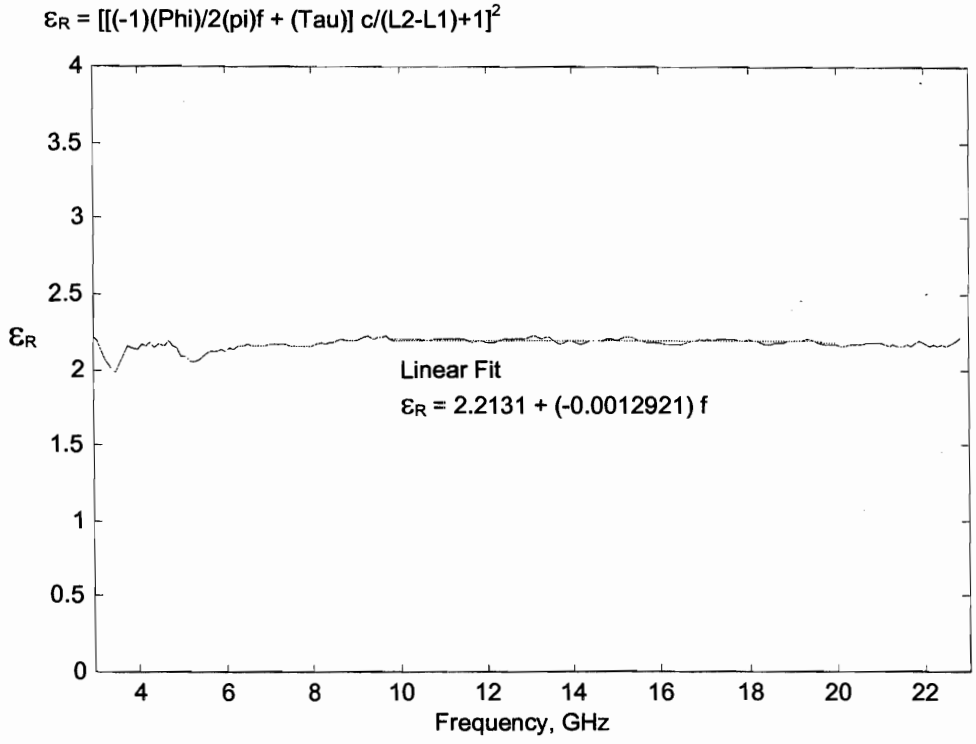

Figure 40. Relative permittivity for type-265 || artificial dielectric material calculated from time domain TEM-cell measurement

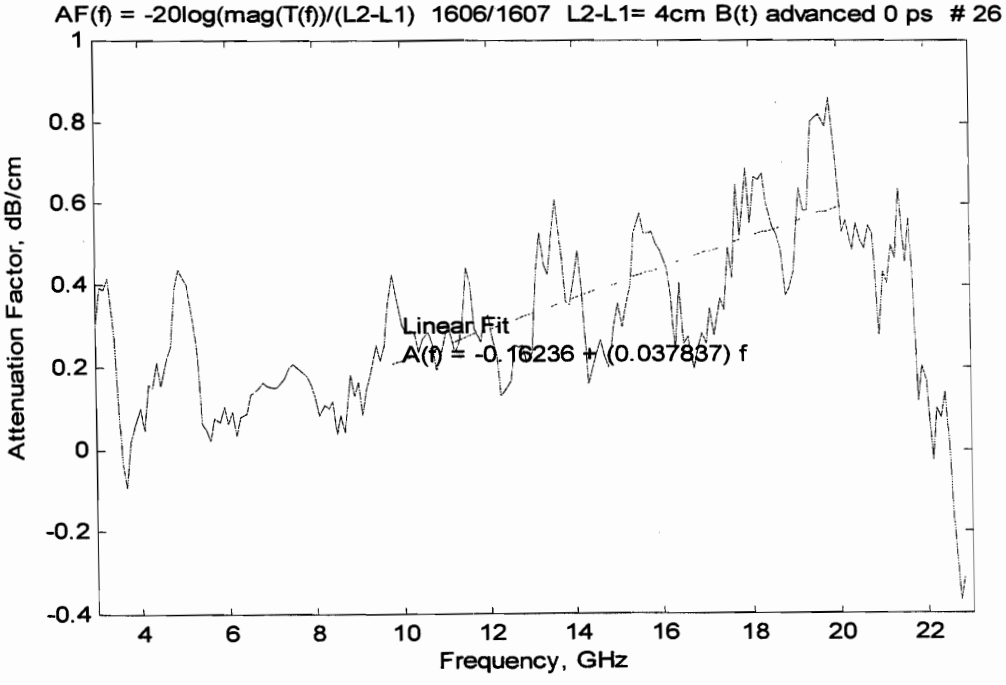

Figure 41. Attenuation factor for type-265 || artificial dielectric material calculated from time domain TEM-cell measurement

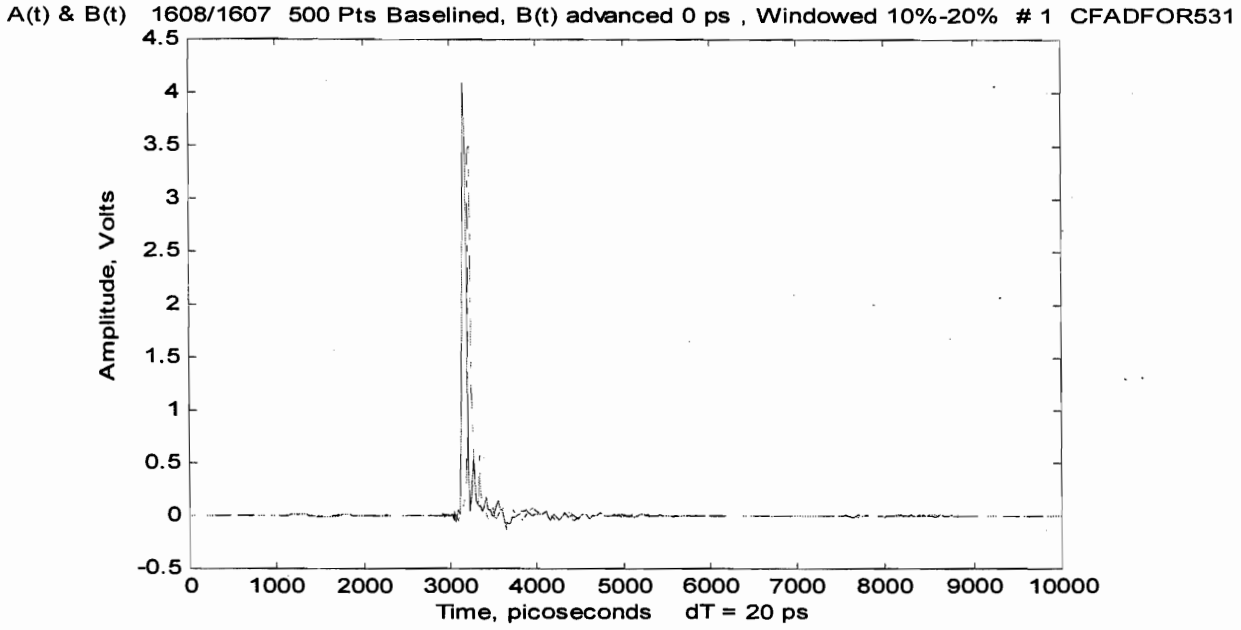

Figure 42. Time domain transmission waveforms A(t) and B(t) for propagation through lengths ℓ_1 and ℓ_2 of type-265 $\perp$ artificial dielectric material in TEM-cell

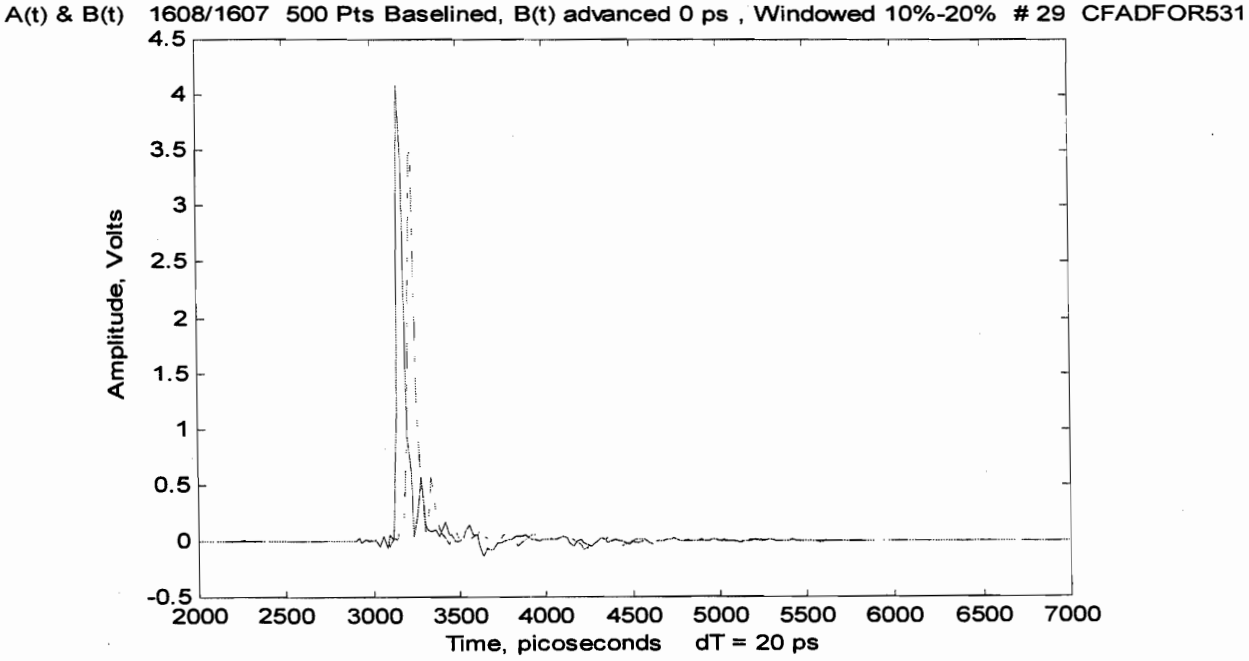

Figure 43. Time domain transmission waveforms A(t) and B(t) for propagation through lengths ℓ_1 and ℓ_2 of type-265 $\perp$ artificial dielectric material in TEM-cell at finer resolution

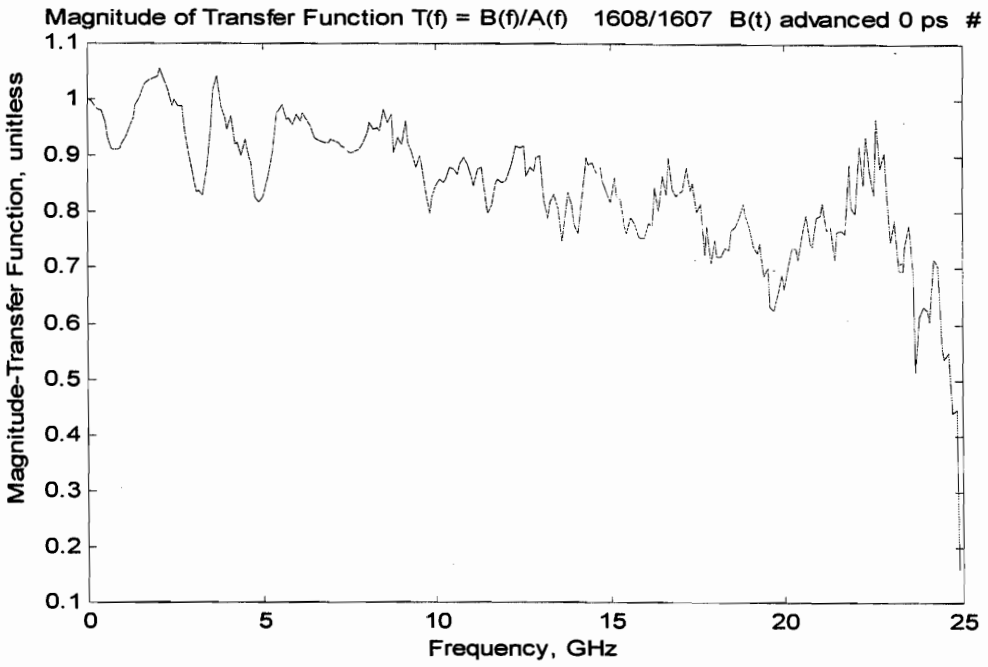

Figure 44. Magnitude of transfer function for propagation through differential length ($\ell_2 - \ell_1$) of type-265 $\perp$ artificial dielectric material in TEM-cell

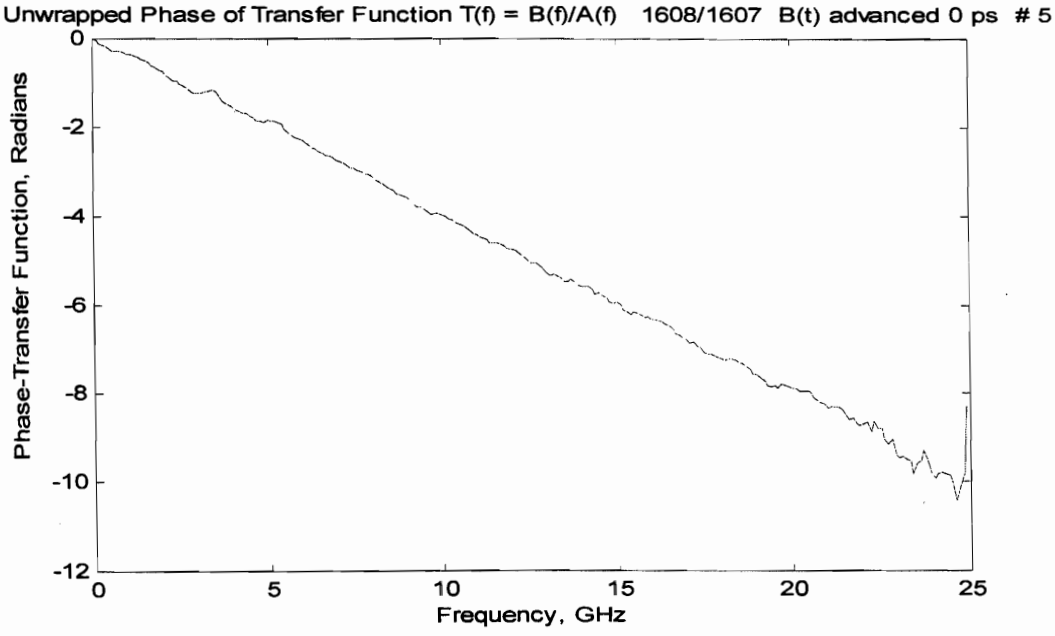

Figure 45. Phase of transfer function for propagation through differential length ($\ell_2 - \ell_1$) of type-265 $\perp$ artificial dielectric material in TEM-cell

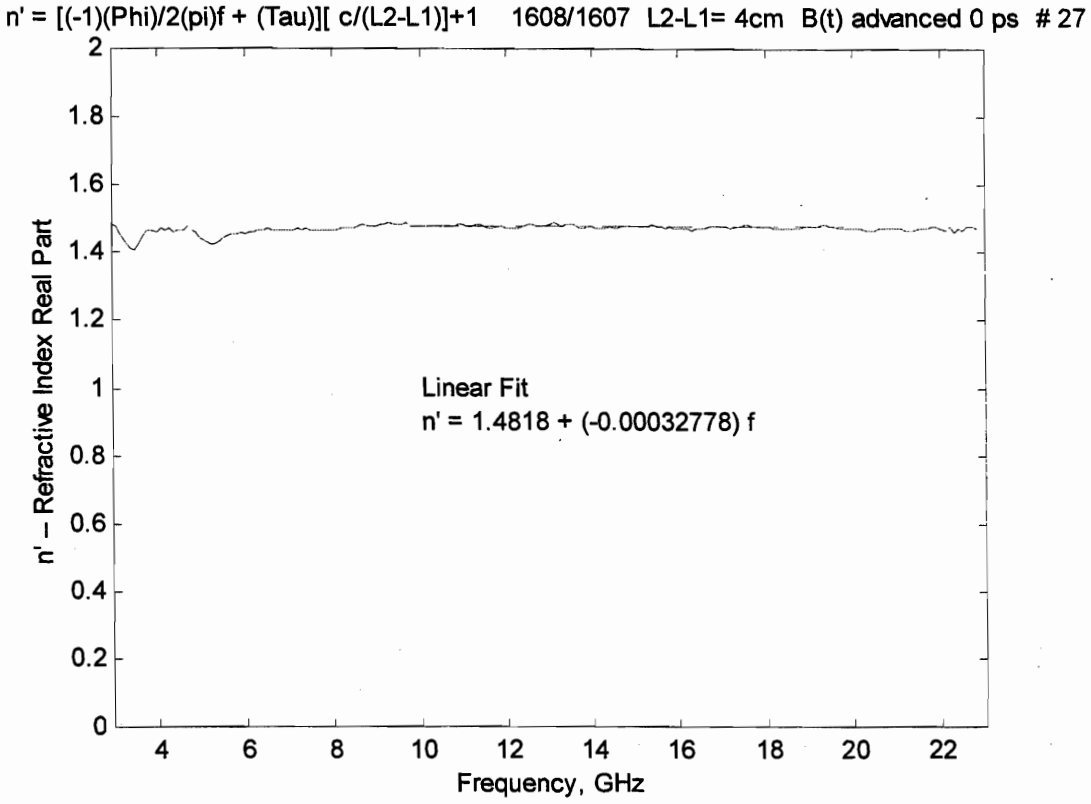

Figure 46. Real part of refractive index for type-265 ⊥ artificial dielectric material calculated from time domain TEM-cell measurement

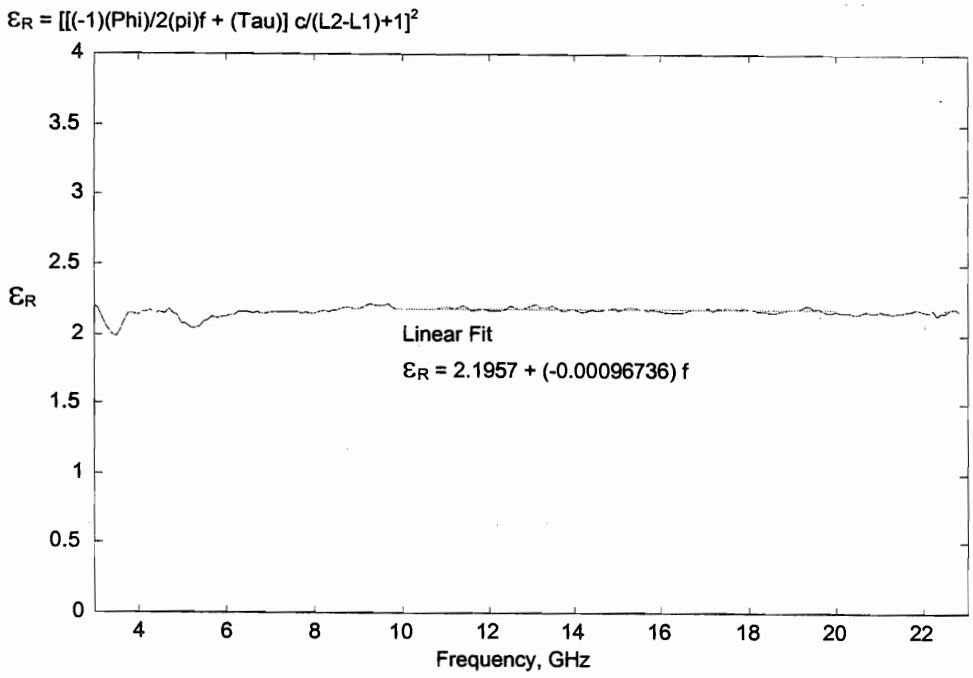

Figure 47. Relative permittivity for type-265 ⊥ artificial dielectric material calculated from time domain TEM-cell measurement

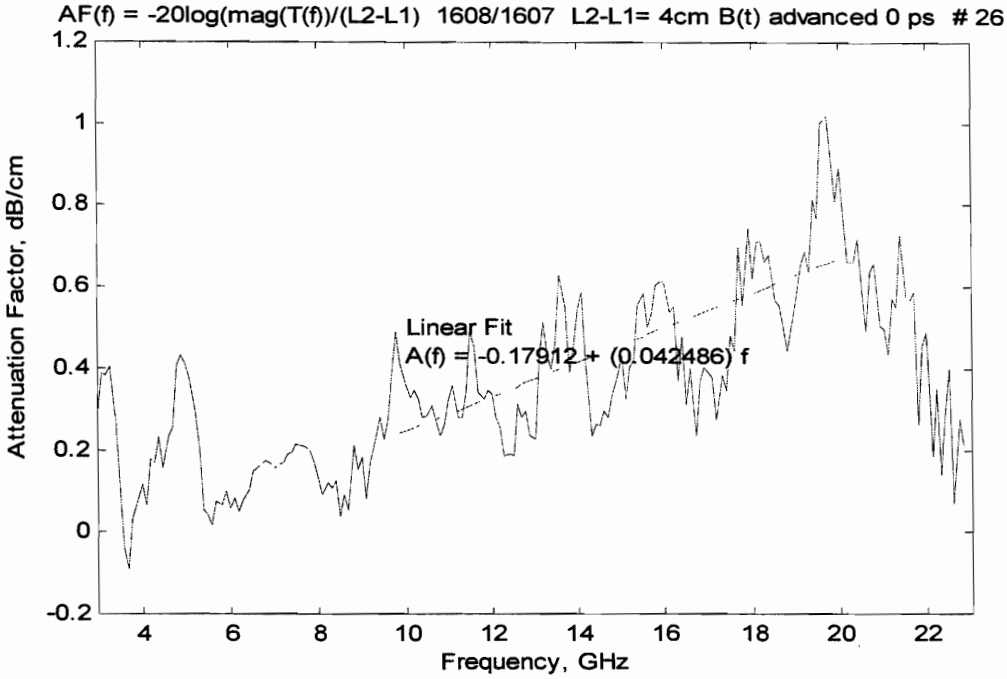

Figure 48. Attenuation factor for type-265 ⊥ artificial dielectric material calculated from time domain TEM-cell measurement

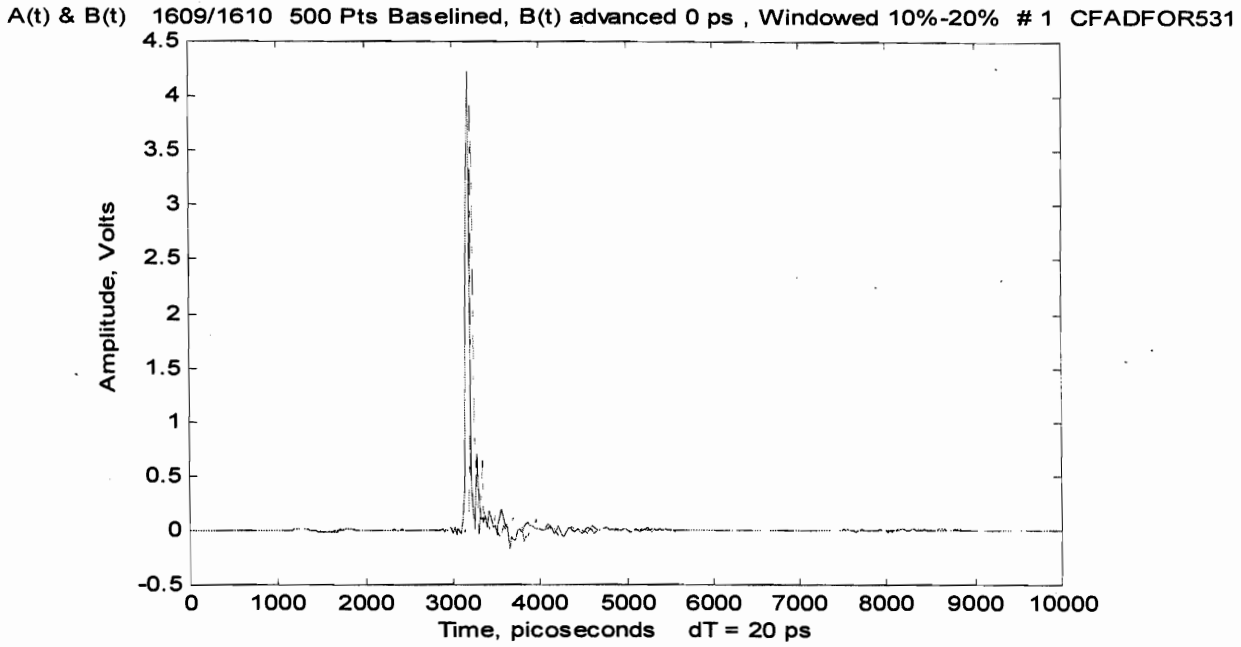

Figure 49. Time domain transmission waveforms A(t) and B(t) for propagation through lengths ℓ_1 and ℓ_2 of type-236 artificial dielectric material in TEM-cell

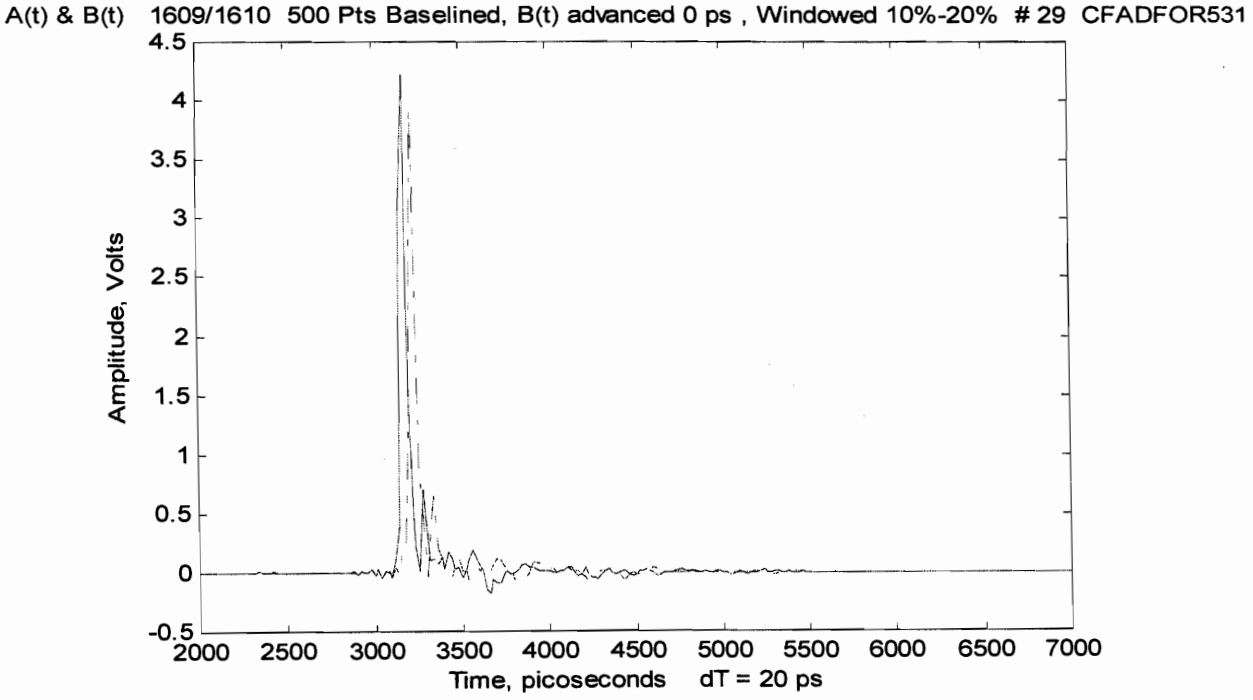

Figure 50. Time domain transmission waveforms A(t) and B(t) for propagation through lengths ℓ_1 and ℓ_2 of type-236 artificial dielectric material in TEM-cell at finer resolution

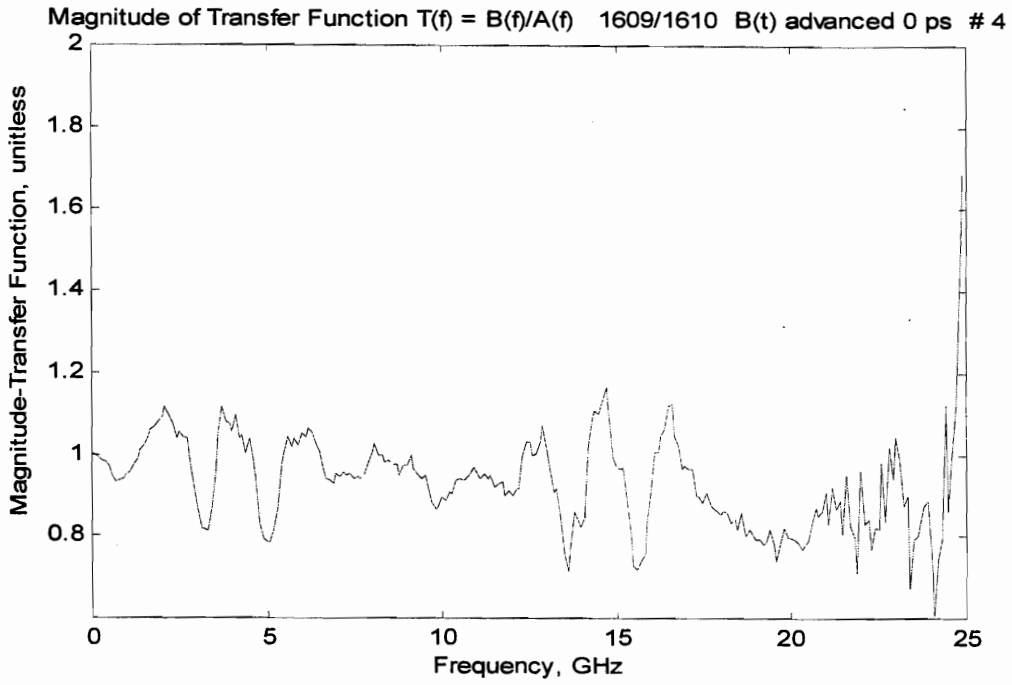

Figure 51. Magnitude of transfer function for propagation through differential length ($\ell_2 - \ell_1$) of type-236 artificial dielectric material in TEM-cell

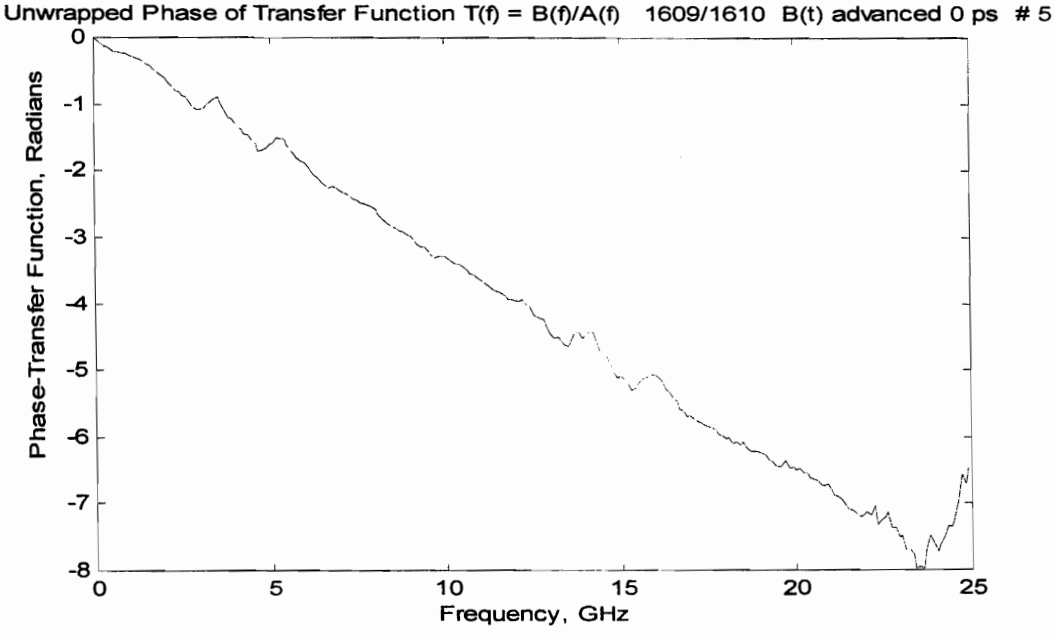

Figure 52. Phase of transfer function for propagation through differential length ($\ell_2 - \ell_1$) of type-236 artificial dielectric material in TEM-cell

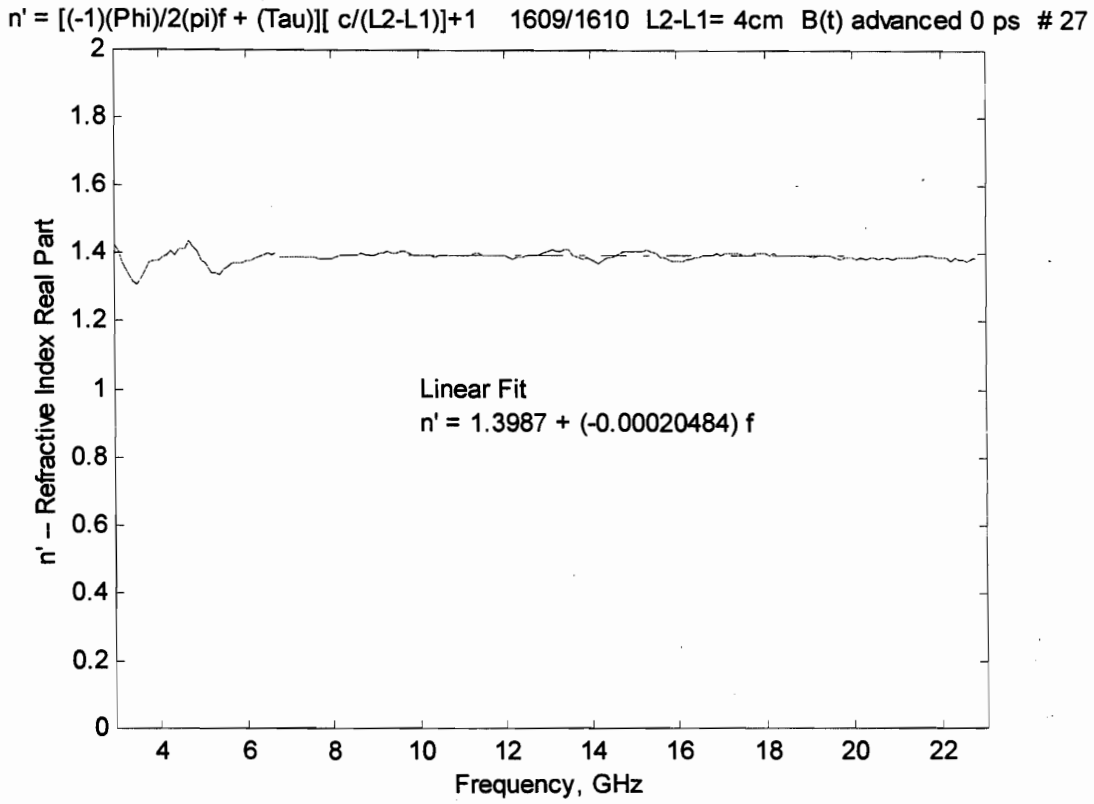

Figure 53. Real part of refractive index for type-236 artificial dielectric material calculated from time domain TEM-cell measurement

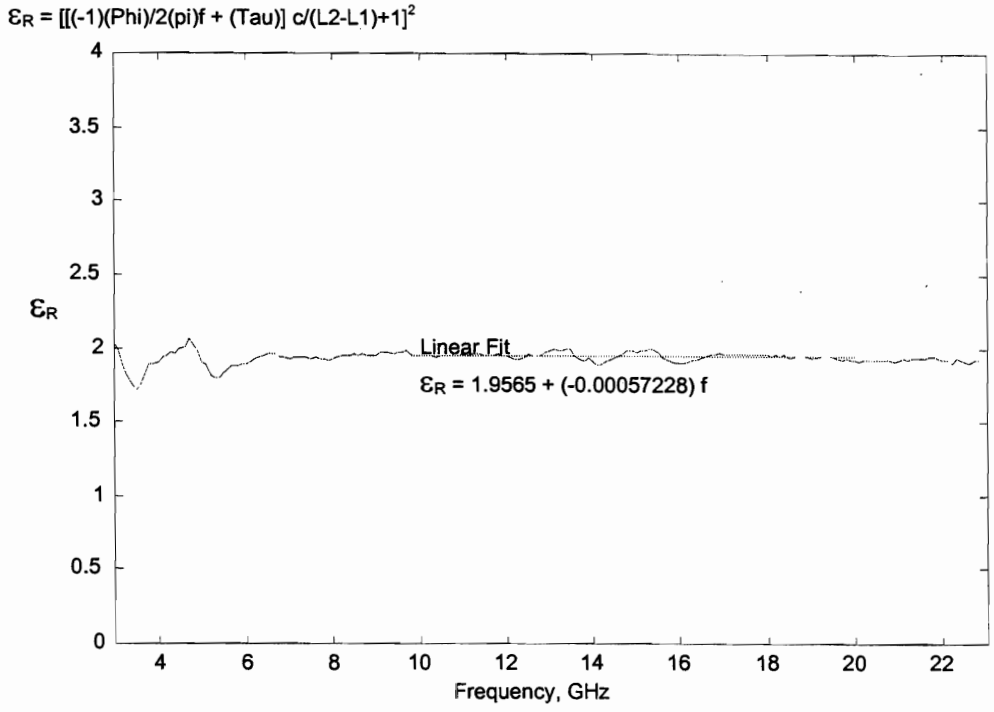

Figure 54. Relative permittivity for type-236 artificial dielectric material calculated from time domain TEM-cell measurement

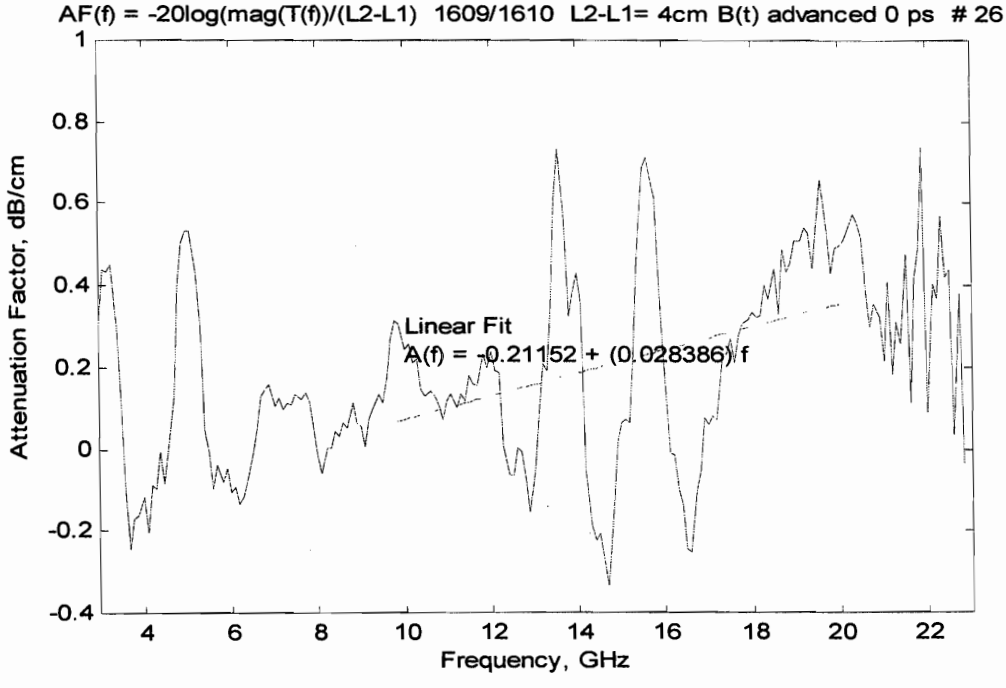

Figure 55. Attenuation factor for type-236 artificial dielectric material calculated from time domain TEM-cell measurement

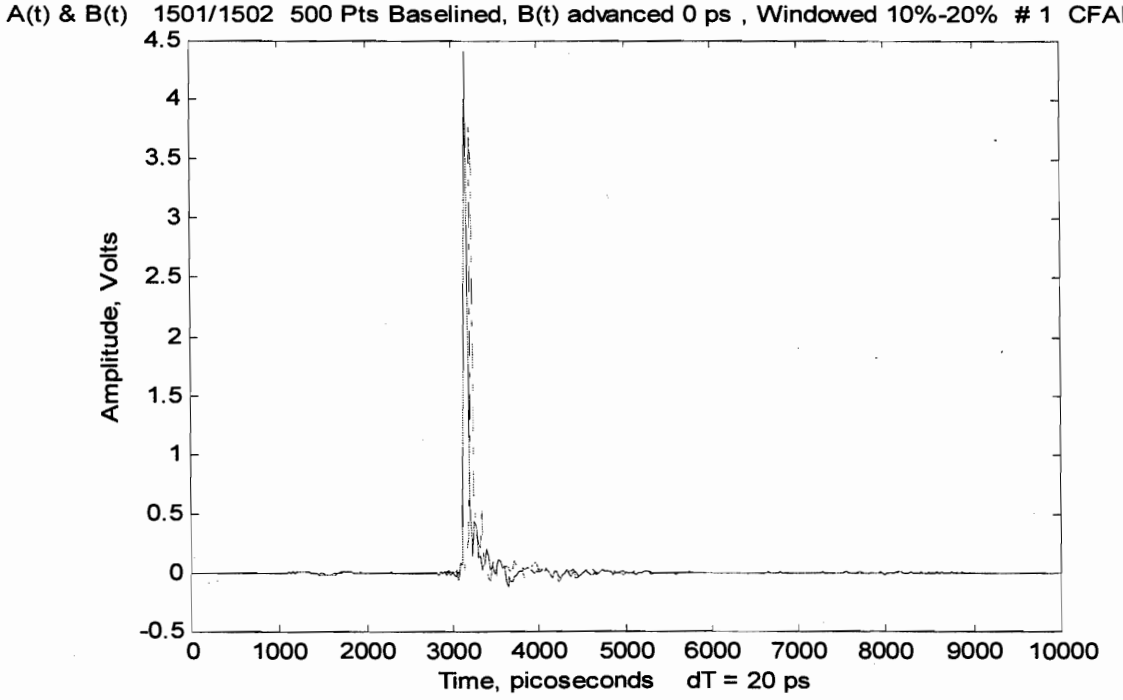

Figure 56. Time domain transmission waveforms A(t) and B(t) for propagation through lengths ℓ_1 and ℓ_2 of polyethylene in TEM-cell

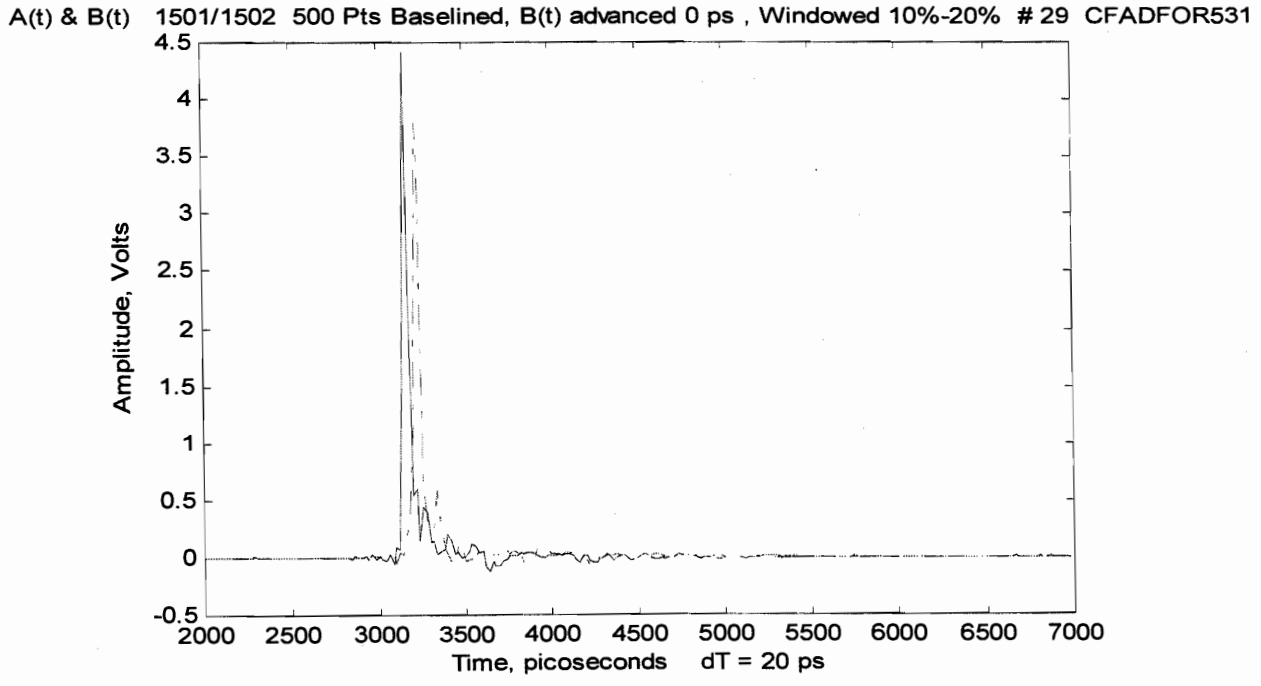

Figure 57. Time domain transmission waveforms A(t) and B(t) for propagation through lengths ℓ_1 and ℓ_2 of polyethylene in TEM-cell at finer resolution

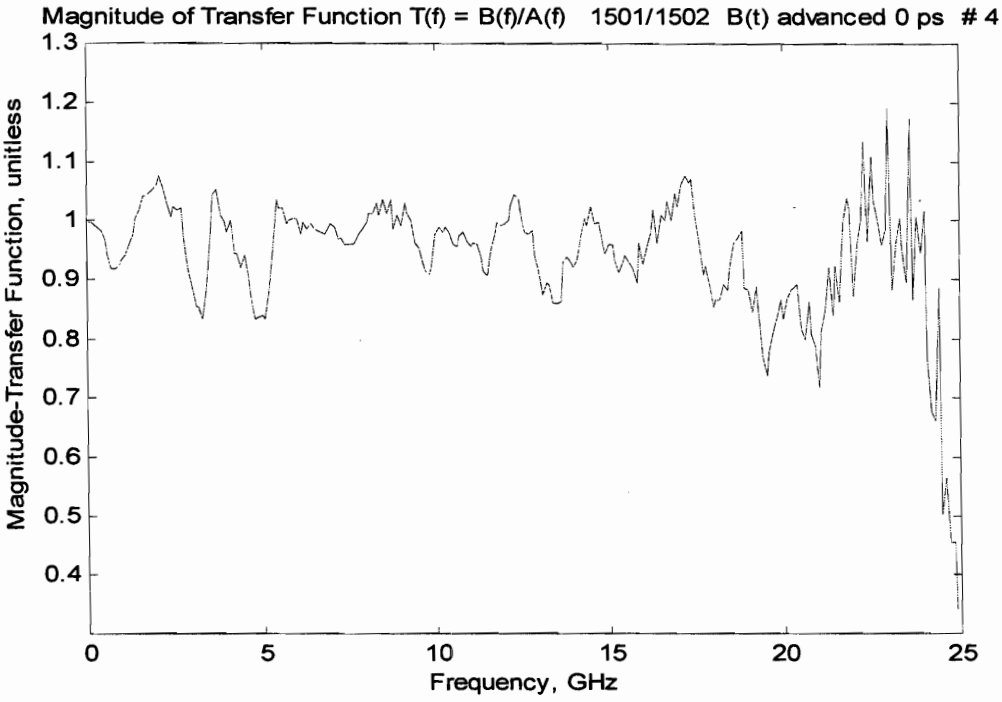

Figure 58. Magnitude of transfer function for propagation through differential length ($\ell_2 - \ell_1$) of polyethylene in TEM-cell

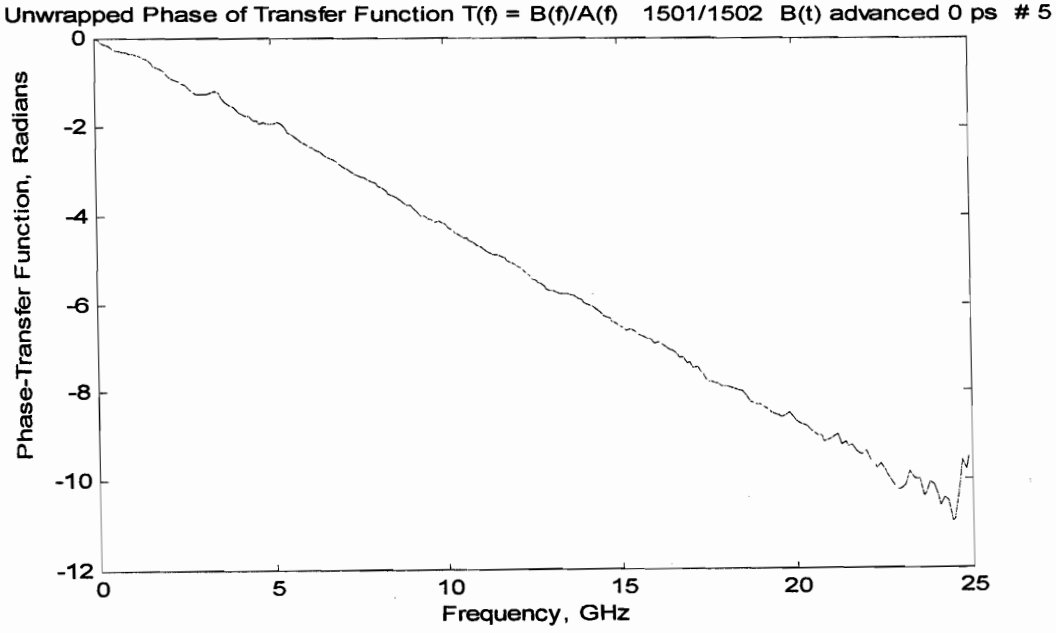

Figure 59. Phase of transfer function for propagation through differential length ($\ell_2 - \ell_1$) of polyethylene in TEM-cell

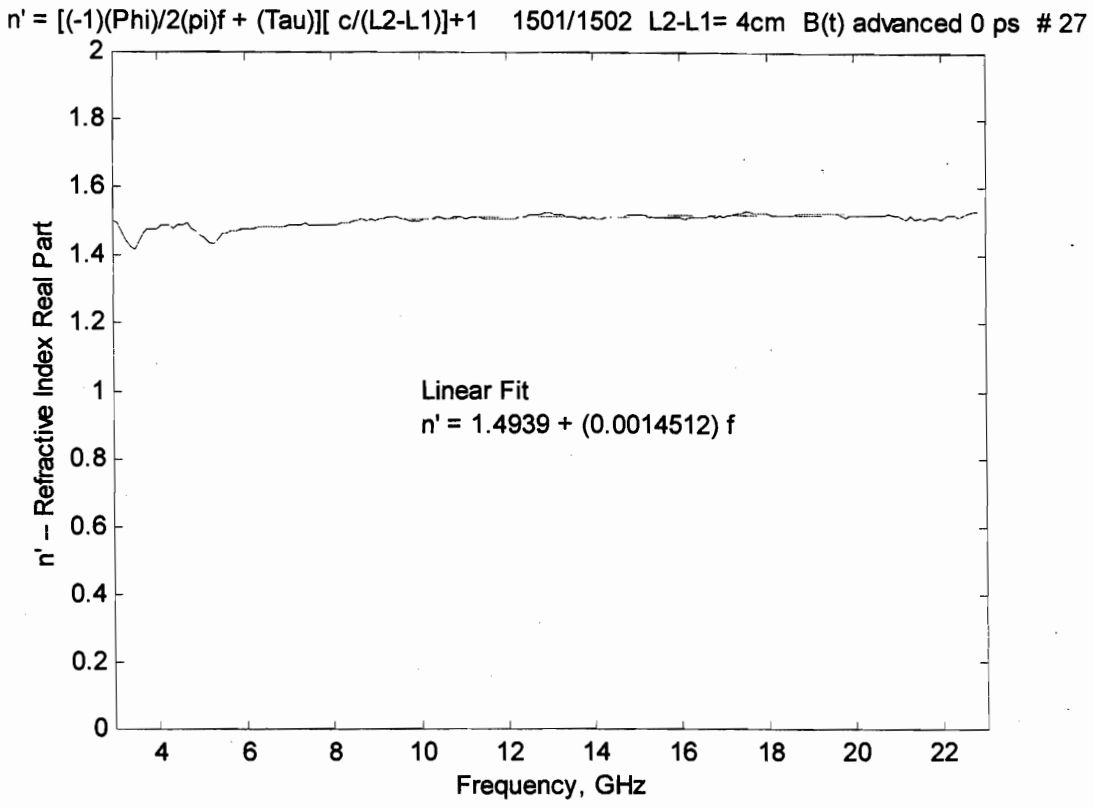

Figure 60. Real part of refractive index for polyethylene calculated from time domain TEM-cell measurement

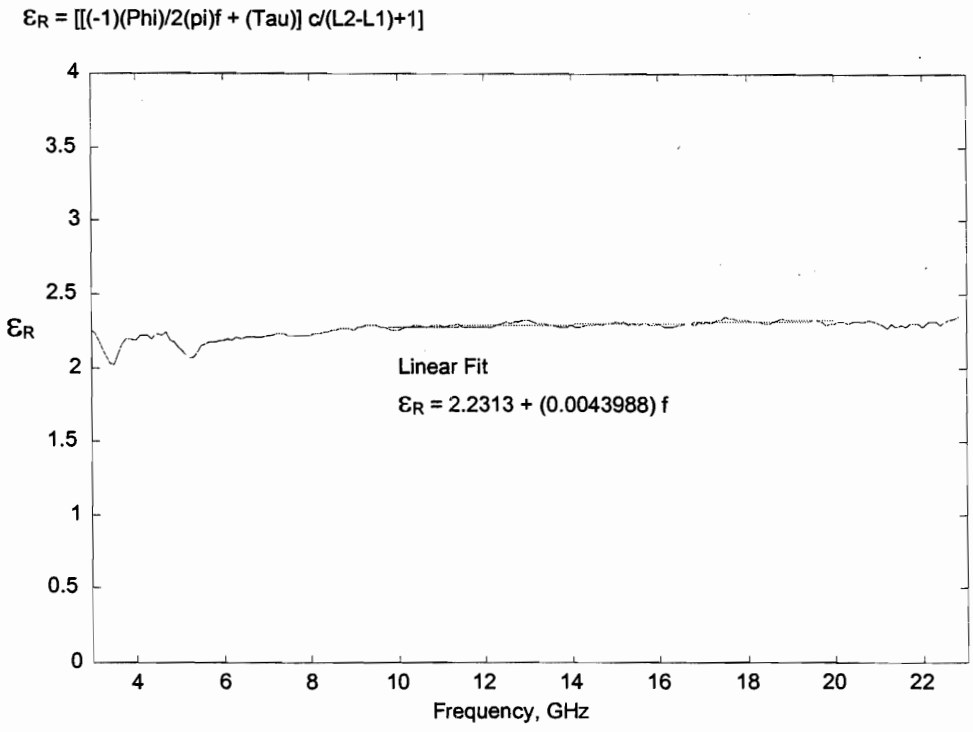

Figure 61. Relative permittivity for polyethylene calculated from time domain TEM-cell measurement

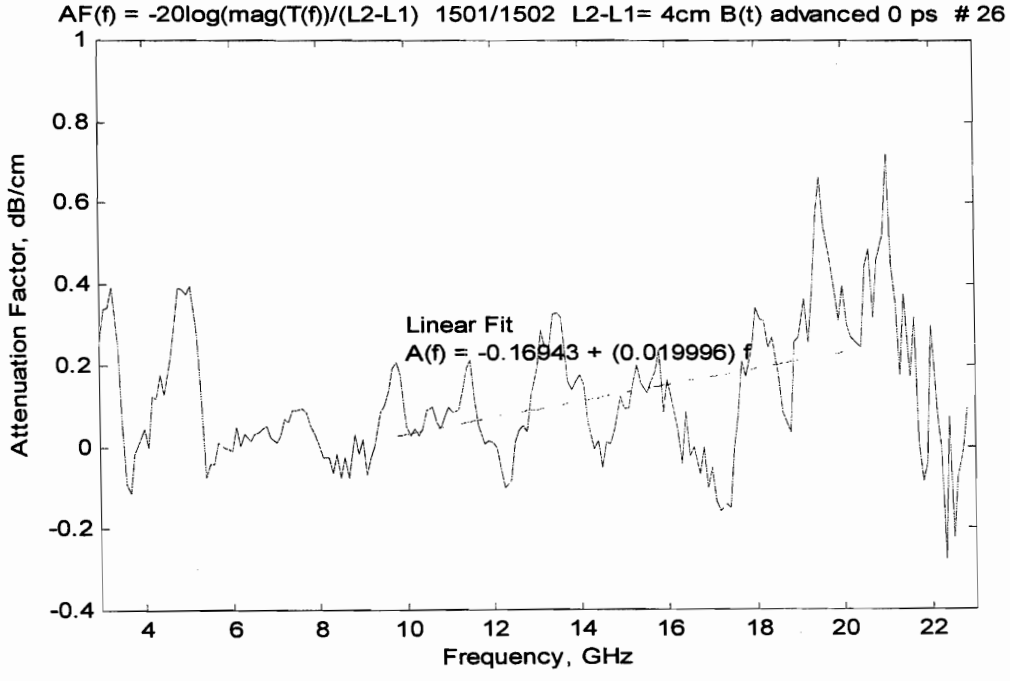

Figure 62. Attenuation factor for polyethylene calculated from time domain TEM-cell measurement

Table 4 summarizes the measured data on the refractive index for each of the materials studied by the bounded wave transmission method using the TEM-cell. In each case, the value of n(f) is calculated for the discrete frequencies using the least squares linear fit equation which is given on the graph of the index for the material.

Table 4. Frequency Dependence of Refractive Index from Fourier Transformed TEM Cell Time Domain Bounded Wave Transmission Data

Real part of refractive index n = c/v as a function of frequency

Material	Frequency			
	2 GHz	5 GHz	10 GHz	20 GHz
type 265 $\parallel$	1.49	1.49	1.48	1.48
type 265 $\perp$	1.48	1.48	1.48	1.47
type 236	1.40	1.40	1.40	1.39
polyethylene	1.50	1.50	1.51	1.52

5. SUMMARY

The results obtained from measurements of the complex dielectric parameters of the artificial dielectric material are encouraging for applications. Both the type 265 and type 236 artificial dielectric material should be useful for the application to dielectric lenses and phase control elements for wideband and ultra-wideband antenna systems. We believe the measurements obtained with bounded waves in the TEM-cell are more accurate since they avoid problems with wave curvature which were seen to be significant for some of the measurements with freely propagating waves. The data summarized by table 4 shows that the artificial dielectric materials give a refractive index which is nearly independent of frequency over a decade bandwidth. The manufacturer specified the permittivity to be 2.5 ±10% for the type 265 material. This would give a refractive index of 1.58. The measured value from the TEM-cell was 1.48 for both polarizations. We consider this to be good agreement for the first batch of an experimental material. The type 236 material, which is even lighter in weight than the type 265, gave a refractive index of 1.40 at mid-band and was also quite flat with frequency over a decade bandwidth.

The attenuation factors were not measured with a high degree of accuracy due to limitation on amplitude stability of the measurement system as discussed in section 3. Nevertheless, it was determined that both type 265 and type 236 material gave low attenuation factor with less than 0.4 db/cm for a mid-band frequency of 10 GHz. The attenuation factor drops linearly with frequency. For lenses of reasonable dimensions, the artificial dielectric material should perform well for frequencies below 10 GHz and may be useful with thin lenses for frequencies beyond 20 GHz.

More precise measurements of attenuation factor may be warranted if operation beyond 10 GHz or lenses greater than 10 cm thick are required. In this case, frequency domain measurements of the dielectric attenuation factor can give more precision. The material properties measured in this work should be adequate for most UWB and WB applications. The data of table 4 should be of sufficient accuracy to allow lenses to be designed using the standard formulas of physical and geometric objects.

We now compare results obtained using bounded waves in the TEM-cell with those obtained using freely propagating waves between two TEM-horn antennas. We compare mid-band values for the refractive index n(f) measured at a frequency of 10 GHz. Comparison of the data in the 10 GHz column on table 4 with that on table 3 shows excellent agreement of the two methods for the polyethylene calibration standard. Both methods give a mid-band refractive index of 1.51 which is in good agreement with the

literature value of 1.50 given by [3]. The simple time delay calculation also gave a value of 1.51 as shown by table 2.

Good agreement was also seen for the type 236 material where the two antenna method gave a value of 1.40, while the TEM-cell method gave a value 1.42 for the refractive index. The measurements with type 265 material did not show good agreement. The two antenna method gave a value of 1.65, while the bounded wave method gave a value of 1.48 for propagation parallel to the preferred axis and also for propagation perpendicular to the preferred axis.

For the case of polyethylene, we had a large (18 inch X 18 inch) sample and were, therefore, able to place the sample far from the antenna aperture without experiencing diffraction from the edges. This was not the case with the type 265 samples which had to be positioned very near the antenna aperture to avoid diffraction from the edges. We attribute the differing values obtained using the two methods for the type 265 material to wave curvature errors caused by locating the sample too close to the aperture. It is also possible that the two type 265 material samples used for the two measurements had a different composition. The samples used with polyethylene and type 236 material were cut from the same block for both measurements. This was not possible with the type 265 material. The samples used for the two measurements were from two different blocks of material, but both blocks were from the same manufacturers batch.

REFERENCES

1. E. G. Farr and C. A. Frost, Time Domain Measurement of the Dielectric Properties of Water in a Coaxial Test Fixture, Measurement Note 49, December 1996.

2. C. A. Frost, et al, Solid State Switched Array Project interim report.

3. A. R. von Hippel, Ed., 1954, *Dielectric Materials and Applications*. Tech. Press of MIT and Wiley, New York.

4. A. M. Nicolson and G. F. Ross, "Measurement of the Intrinsic Properties of Materials by Time-Domain Techniques", IEEE Trans., Instrumentation and Measurement, Vol. IM-19, No. 4, November 1970, PP. 377-382.

5. C. Courtney, W. Motil, T. Bowen, and S. Blocher, Measurement Methods and the Characterization of the Electromagnetic Properties of Materials, Measurement Note 48, December 1996.

6. J. F. Aurand, Measurements of Transient Electromagnetic Propagation Through Concrete and Sand, Sandia Report, SAND96-2254, September 1996.

7. E. G. Farr and C. A. Frost, Impulse Propagation Measurements of the Dielectric Properties of Water, Dry Sand, Moist Sand, and Concrete, Measurement Note 52, November 1997.